

Numerical analysis of a helical spiral microevaporator-microreformer system for enhanced methanol conversion and hydrogen production

Devendra Yadav^a, Xinlong Lu^a, Prabhat Dansena^b, Dengwei Jing^{a,*}

^a State Key Laboratory of Multiphase Flow in Power Engineering, Xi'an Jiaotong University, Xi'an, Shaanxi, 710049, PR China

^b Department of Computer Science Engineering, C V Raman Global University Bhubaneswar, Odisha, 752054, India

ARTICLE INFO

Keywords:

Hydrogen
Steam reforming
Methanol
Microreactor
Catalyst
Helical spiral

ABSTRACT

The study aims to simplify microreactor system design by eliminating the need for a separate evaporator unit while enhancing microreactor performance. This study comprehensively elucidates the transition of fed liquid methanol and water mixture species conversion within this coupled system. The behavior and performance of this coupled system are investigated across variations in reaction parameters, including steam to methanol ratio (S/C ratio=1–3), applied heat flux ($q = 100\text{--}900\text{ W/m}^2$), and variations in $\text{CuO/ZnO/Al}_2\text{O}_3$ catalyst thicknesses ($37.5\text{ }\mu\text{m}\text{--}75\text{ }\mu\text{m}$) coated onto the wall. The study demonstrates that methanol steam reforming, an endothermic reaction, leads to substantial temperature drops as vapor moves from the microevaporator to the microreformer, balancing the heat supplied and absorbed in the mixture. The temperature range of $225\text{--}250\text{ }^\circ\text{C}$ was found to be critical for complete methanol conversion, with higher heat flux and S/C ratios enhancing conversion rates. Thin catalyst layers in the helical design allow for rapid methanol conversion, while thicker layers result in higher hydrogen (H_2) production rates. Pareto front analysis identifies design D4 ($\Delta t = 37.5\text{ }\mu\text{m}$) as optimal, requiring a minimum heat flux of 300 W/m^2 and an S/C ratio of 1 to achieve an H_2 flow rate per unit catalyst weight (r_{H_2}) of 0.034 and 99.4 % methanol conversion performance.

1. Introduction

The increasing energy demand has placed significant pressure on fuel consumption to meet this growing need. With current energy reliance heavily centered on fossil fuels, concerns regarding air pollution have surged to the forefront of public discourse. This has sparked a pressing need for sustainable energy alternatives that can mitigate environmental impact while ensuring a reliable energy supply for the future [1]. This has prompted both the power sector and governing bodies to explore alternatives to fossil fuels, leading to substantial investments in renewable energy sources such as solar, wind, tidal, hydro, geothermal, and biomass. These renewable energy sources have the potential to mitigate carbon emissions, but they also face challenges such as high costs, their intermittency nature, the need for significant investment, and inefficient storage systems [2,3]. These obstacles hinder the full utilization of renewable energy. However, H_2 fuel presents a promising and sustainable solution for the future. H_2 has the potential to address current environmental challenges stemming from fossil fuel use, as it is a clean energy source that produces only water vapor as a byproduct [4,5].

The transportation sector is the second-largest energy consumer globally, heavily reliant on fossil fuels, and a significant contributor to environmental damage [6]. H_2 fuel has the potential to play a crucial role in revolutionizing the transportation sector. Despite the growing interest in battery-based electric vehicles over the past decade, such vehicles still face numerous challenges and limitations compared to fossil fuels. Key challenges with electric vehicles include low energy density, long charging times, limited power storage capacity, battery lifespan, and low driving range [7,8]. The proton exchange membrane fuel cell (PEMFC), powered by H_2 , presents a promising alternative to both battery and fossil fuel-based engines [9]. Research indicates that PEMFCs boast significantly higher energy density compared to batteries [10]. The PEMFC also offers rapid response, fast startup, long driving range, lightweight construction, and produces clean exhaust gases [11]. However, current PEMFC-based vehicles face several challenges, including cost, storage, and infrastructure requirements for H_2 , which are considerable and contribute to the limited market penetration of fuel cell vehicles [12]. The primary challenge lies in the cost of H_2 production, storage, and its transportation. At present, there are several ways to

* Corresponding author.

E-mail addresses: devendra.yadav@stu.xjtu.edu.cn (D. Yadav), xinlonglu@stu.xjtu.edu.cn (X. Lu), p.dansena23@gmail.com (P. Dansena), dwjing@mail.xjtu.edu.cn (D. Jing).

<https://doi.org/10.1016/j.cep.2024.110149>

Received 24 September 2024; Received in revised form 9 December 2024; Accepted 30 December 2024

Available online 1 January 2025

0255-2701/© 2024 Elsevier B.V. All rights are reserved, including those for text and data mining, AI training, and similar technologies.

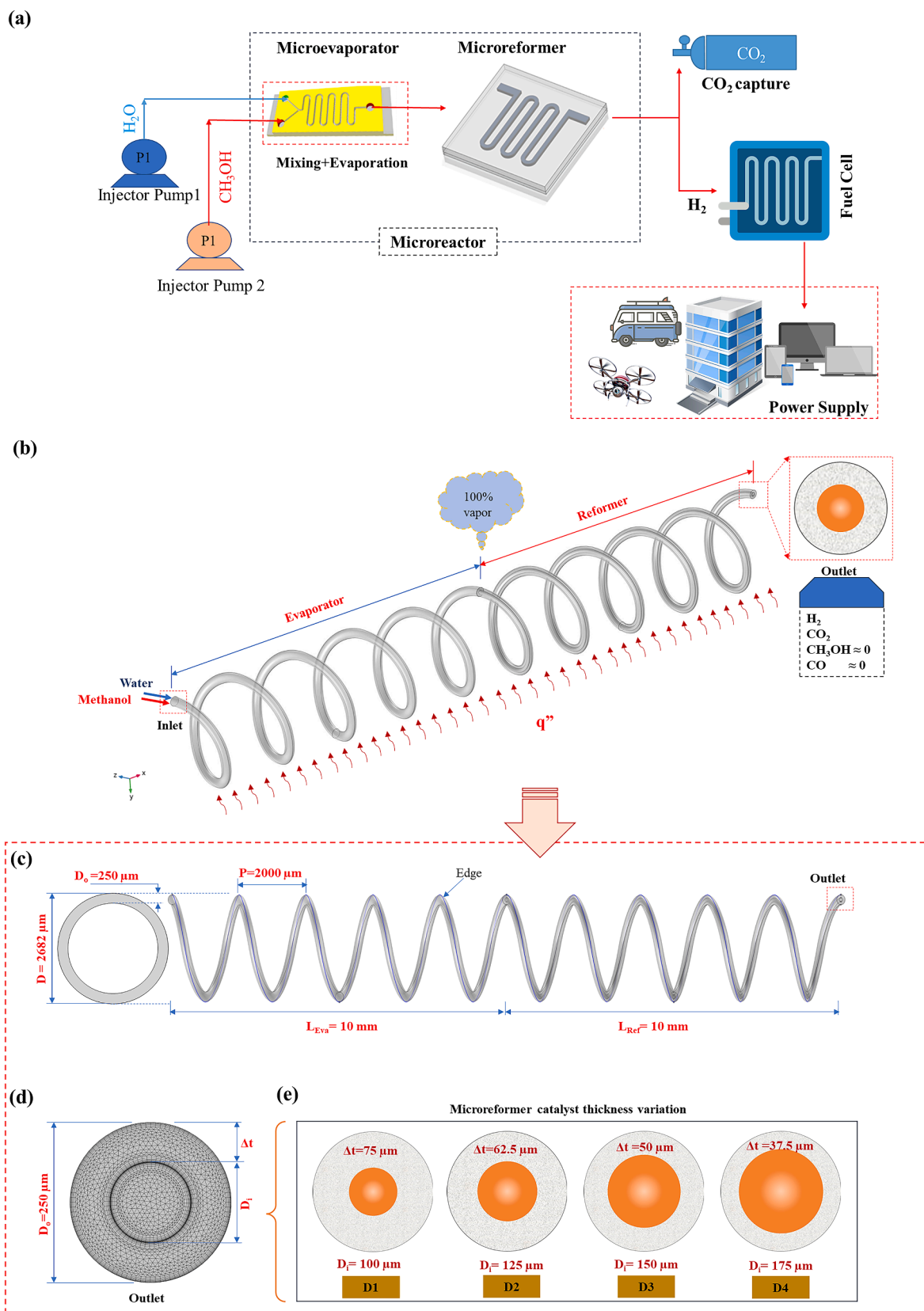


Fig. 1. (a) Microevaporator-microreformer system for methanol steam reforming to meet energy needs, (b) Helical spiral microevaporator-microreformer coupled design for steam reforming, (c) Microevaporator and microreformer size, (d) Outlet of microreformer with the structured mesh, (e) Microreformer designs with four catalyst thicknesses.

produce H_2 , broadly classified based on energy processes such as thermal [13], photonic [14], electrical [15], and biochemical [16]. Currently, the conventional thermal pathway method of steam reforming accounts for 90 % of global H_2 production [17]. Steam reforming utilizes hydrocarbons, primarily natural gas, for the reforming process. This H_2 production method still heavily rely on conventional reactors, which, despite being one of the cheapest ways to produce H_2 compared to other methods, do not offer cost-effectiveness for transportation when compared to fossil fuel-based vehicles. Other disadvantages include being less efficient, and steam reforming from these reactors is also concerning for the environment, necessitating additional carbon removal units [18]. This steam reforming process is highly energy-intensive due to the endothermic nature of the reaction, requiring temperatures of 800–1000 °C [19]. To achieve these temperatures, part of the gas is combusted, constituting approximately 20 % of the total consumption [20]. This combustion releases CO_2 and nitrogen oxides (NO_x). Addressing the inefficiencies, high costs, environmental impacts, and complexities of storage and transportation in the current H_2 production system is crucial.

Onboard H_2 production has emerged as a potential solution to these challenges. Microreactor technology is key to onboard H_2 production from different hydrocarbon fuels. Fig. 1(a) illustrates the utilization of microreactors for methanol steam reforming to fulfill energy needs across different applications. Microreactors are miniaturized reaction systems characterized by dimensions in the submillimeter range [11]. Coupled with fuel cells, microreactors hold potential as a promising energy source to power various electronic devices, particularly in the transportation sector [21]. Microreactor systems offer several advantages over conventional reactors, including compactness resulting in lower weight, high catalyst loading per unit volume, enhanced heat and mass transfer, increased efficiency, precise reaction control, featuring utilization of different hydrocarbons, and reduced operational costs [22–26]. Among various hydrocarbons for onboard H_2 production, methanol-based steam reforming in a microreactor appears particularly promising due to several advantages associated with methanol utilization [27]. Methanol is highly compatible with this purpose due to its high energy density, high H_2 to carbon ratio, low reforming temperature (200–350 °C) [28], ease of handling and storage, and its function as a H_2 carrier for PEM fuel cells [29]. Additionally, methanol can be produced from both renewable and non-renewable carbon sources such as natural gas, coal, biomass, or from flue gas CO_2 emitted from coal power plants [25]. The PEM fuel cell requires a CO concentration below 20 ppm [11], this limit can be achieved with methanol steam reforming. In the future, methanol-based microreforming coupled with fuel cells could potentially replace lithium-ion batteries.

Typically, a microreactor consists of an evaporator chamber and a reformer chamber. The fuel feed first enters the evaporator chamber, where it undergoes complete vaporization. Subsequently, the produced mixture vapor of methanol and water enters the microreformer chamber for the steam reforming reaction, as depicted in Fig. 1(a) [30]. Chu et al. [31] proposed a thermocouple system design integrating evaporator chamber, reforming chamber, and heating system, where heating was provided through rods. This configuration was aimed at facilitating methanol evaporation and subsequent reforming. Expanding on this concept, Zheng et al. [32] examined a coupled microreactor system consisting of an evaporation chamber, a mixing chamber for air and methanol, and a reaction chamber for combustion and reforming. In their design, methanol was evaporated, mixed with air, and then reacted in the combustion chamber to supply heat required for reforming in the reformer chamber. Yoshida et al. [33] introduced a microreformer system that coupled a microchannel evaporator with a catalyst support chamber. The system was vertically structured, with the combustion chamber operating at 280 °C located above the reformer, while the evaporator at the bottom operated at 120 °C. This study focused on the effects of combustion power and fuel feed rates on the concentrations of CO and H_2 . Under optimal conditions, with a combustion power of 11 W,

the system produced H_2 with a low heating value (LHV) of 5.9 W. Wang et al. [34] developed a methanol steam reforming microreactor for H_2 production to power a Low Temperature PEMFC. The system design incorporates multiple microreactors and consists of several aluminum plates that form distinct chambers for combustion, evaporation, and reforming. The reformer chamber accommodates a higher catalyst loading, thereby enhancing H_2 production. In the developed system, a methanol conversion rate of 93 % was achieved, with an energy efficiency of 76.2 %. When integrated with the fuel cell, the system is capable of generating up to 160 W of electricity.

Over the last two decades, numerous studies have focused on enhancing the performance of microreactors. Researchers in this field have proposed various designs and investigated both the structural and reaction parameters aimed at achieving the high performance of microreactor. Literature surveys indicate that structural modifications lead to improved microreactor performance [9,35]. In this context, Zhuang et al. [36] conducted numerical investigations on syngas production through methanol steam reforming using a multichannel reactor. Researchers explored the impact of parameters such as S/C ratio, weight hourly space velocity, and catalyst layer thickness on reactor performance. Their research showcased that the proposed design achieved an impressive 89.65 % methanol conversion. Moreover, the findings revealed that in the proposed reactor design, there was only a maximum temperature difference of 2.5 °C, indicating better thermal distribution within the reactor.

Thermal management is critical for maintaining stable reactions and optimal performance in microreactors. Hu et al. [37] demonstrated that thermal matching between the combustor and reactor sides can lead to the formation of hot spots when the feed enters the channel. This underscores the importance of effective thermal management, which can be achieved through the proper distribution of the feed to ensure uniform heat transfer and stable operation. In the study by Chen et al. [35], numerical simulations were conducted on a tree-shaped structure of a microreactor for methanol steam reforming, aiming to optimize flow and enhance performance compared to the serpentine structure. The proposed tree-shaped design improves the flow distribution of reactants and provides a larger surface-to-volume ratio. Additionally, the reduced velocity at the branches of the tree-shaped reactor leads to higher conversion rates compared to the serpentine-shaped microreactor, albeit with the same pressure loss. Chen and Yu [38] performed a numerical analysis of a square-section multichannel microreactor designed for methanol steam reforming. Their study investigated transport phenomena, focusing on the effects of washcoat thickness, channel height, temperature, and flow conditions. The results revealed that increasing the washcoat thickness reduces the reaction rate, primarily due to diffusion limitations of reactant molecules. They also highlighted the importance of carefully selecting flow velocity to optimize both methanol conversion and H_2 yield. For the studied design, a maximum power output of 70 W per channel was achieved. To further enhance transport processes, Chen [39] introduced hemispherical protrusions along the channel walls. These modifications significantly improved reaction rates and throughput by intensifying transport phenomena. Additionally, the enhanced design ensured an energy balance between the exothermic and endothermic reactions, which is crucial for efficient H_2 production from methanol. The H_2 production performance of microreactor systems is strongly influenced by the flow field, which is directly linked to the channel structure and catalyst support. As discussed earlier, a well-optimized channel structure and proper feed distribution can significantly increase the specific surface area, thereby improving heat and mass transfer efficiency [40]. Similarly, Wang et al. [41] demonstrated that, in a microtubular reactor, poor heat transfer within packed-bed catalysts can be mitigated through proper temperature distribution. By utilizing fins on the combustion-side tube, the maximum temperature difference within the same section was reduced by 80.7 %, underscoring the importance of thermal management and structural optimization for enhanced microreactor performance.

In the study on catalyst effects, Hafeez et al. [25] demonstrated that catalyst particle size has a negligible effect on methanol steam reforming. However, the results also indicated that increasing temperature and residence time resulted in higher methanol conversion rates. In the work of Kim & Kwon [42], a comparison was conducted between a catalyst-coated microreactor and a packed - bed microreactor for the reforming reaction of methanol. The results demonstrated that the catalyst-coated microreactor exhibited higher conversion rates compared to the packed - bed microreactor. The difference was attributed to the heat and mass transfer limitations inherent in the packed - bed microreactor. The work by Chen and Li [43] showed that high-thickness catalyst material reduces the resulting temperature and fuel conversion. In the field of microreactors, copper-based catalysts are widely regarded as the most suitable for methanol steam reforming. One of the popular catalyst compositions used for this process is Cu/ZnO/Al₂O₃, where Cu serves as the main component [44].

The *S/C* ratio is another crucial reaction parameter that significantly affects the steam reforming process in microreactors. Typically, for steam reforming a *S/C* ratio above 1 is considered suitable as it allows for higher fuel conversion. However, a high *S/C* ratio is favored for steam reforming as the reaction progresses, resulting in high conversion and ensuring full conversion of CO to CO₂. However, the appropriate *S/C* ratio selection also depends on the type of fuel utilized for steam reforming [45]. In the study by Chen et al. [46], the effect of the *S/C* ratio on methane steam reforming was investigated. Researchers observed that increasing the *S/C* ratio favored higher conversion but decreased H₂ yield. Conversely, the research also suggested that a low *S/C* ratio could provide higher power even at low temperatures. A similar observation was found in the work of Baydir and Aras [47] on microchannel reactors for methanol steam reforming. It was observed that an increase in the *S/C* ratio resulted in a decrease in H₂ yield while methanol conversion increased. Furthermore, research has indicated that, at a given *S/C* ratio, increasing temperature leads to higher CO selectivity and conversion [48]. This suggests the importance of optimizing the *S/C* ratio.

Temperature plays a critical role in steam reforming processes as it directly impacts reaction efficiency. The temperature of the mixture in steam reforming is closely tied to the heat supplied. Therefore, an efficient design that promotes rapid heat transfer within the reformer is essential for optimal performance. It is important to note that the design of the microreactor is crucial, as it impacts the flow of the mixture, ultimately affecting temperature distribution inside the microreactor [49]. The research demonstrated that increasing temperature leads to higher reaction rates [50], resulting in improved conversion [51]. Higher temperatures also favor H₂ production [47]. Additionally, materials with high thermal conductivity are desirable to maintain uniform temperature distribution and prevent hotspots [52,53]. In the work by Qian et al. [54] it was demonstrated that electric heating enables quick reactor startup.

The literature highlights that methanol steam reforming in microreactors is influenced by both structural and reaction parameters. Consequently, identifying optimal conditions that achieve high performance at minimal cost is crucial. To address such multi-objective challenges in reaction engineering, researchers have employed methods like the Technique for Order of Preference by Similarity to Ideal Solution (TOPSIS) [55], Pareto front solutions, and Genetic Algorithms (GA) [56]. Multi-Objective Optimization has shown significant potential across diverse engineering fields in recent years. Examples include the optimization of food-energy-water systems [57], sustainable power generation for zero emissions [58], and automotive seat frames using machine learning [59]. Other applications involve laser-based optimization of fuel filter parameters [60], integrated energy systems combining electricity, gas, and heat [61], lithium-ion battery cooling systems [62], and kinetic modeling with Bayesian optimization [63]. These examples demonstrate that optimization techniques are versatile and not confined to specific engineering fields. Tang et al. [64] explored

the use of high-temperature exhaust gases for on-line H₂ production as a solution to the challenges of H₂ storage and transportation for engines. In their study, the researchers employed a combination of Response Surface Methodology (RSM) and Multi-Objective Particle Swarm Optimization (MOPSO) to optimize reactor performance. The optimal solution was identified using a Pareto optimal front and further evaluated with the TOPSIS method. Under the optimized conditions - exhaust temperature of 585.21 K, exhaust flow rate of 0.0097 kg/s, *S/C* ratio of 1.48, and a weight hourly space velocity of 1.2, the reactor achieved a H₂ yield of 68.53 mol/h, 83 % methanol conversion, low CO selectivity (0.011), and 21.92 % exhaust energy recovery.

The evaporator serves as the initial component of the microreactor, facilitating the complete evaporation of methanol and water before feeding the mixture into the microreformer. The literature survey revealed that, in the field of microreactors, researchers have primarily focused on microreformers. There is a lack of studies on coupling evaporators with microreformers. This gap in research, particularly concerning microevaporators, can be attributed to the assumption made in CFD simulations that the incoming methanol-water mixture is in the gaseous phase [65]. Additionally, the complexity involved in dealing with both liquid and gaseous phases in reactions contributes to this gap in research. This work presents the first study to introduce a coupled system of a microevaporator and microreformer, streamlining the microreactor setup by eliminating the need for a separate evaporator unit. The comprehensive CFD model developed here provides valuable insights into integrating a microchannel evaporator with a reformer. Additionally, the use of a helical spiral design for the microreactor, as demonstrated in this study, is novel and has not been previously explored, making this research distinctive. The study investigates the performance of helical spiral microreactor by varying the thicknesses of a CuO/ZnO/Al₂O₃ catalyst layer (37.5 μm to 75 μm) coated onto the microreformer's wall, along with different operating parameters heat flux ranging from 100 to 900 W/m² and *S/C* ratio from 1 to 3. In the numerical study, parameters such as mole fraction of products, H₂ flow rate per unit catalyst weight (*r*_{H₂}), and temperature from the steam reforming are assessed to evaluate performance. The present study demonstrates that the proposed coupled system using a helical spiral design microreactor enables faster conversion rates, achieving 100 % methanol conversion over a shorter length of the microreformer. Additionally, this design exhibits superior performance compared to other designs for rapid fuel conversion. In this coupled system, an interesting finding is that with smaller catalyst thicknesses, conversion can initiate even before the methanol and water vapor mixture enters the microreformer, especially under high heat flux conditions. Furthermore, the high catalyst thickness design yields a higher *r*_{H₂} compared to the design with smaller thicknesses. A Pareto front analysis was conducted to optimize methanol conversion, *r*_{H₂}, and pressure drop, with pressure drop treated as a minimization objective by assigning a negative value to convert it into a maximization case. Design D4 emerged as the optimal solution, offering reduced catalyst usage, a lower pressure drop, and enhanced methanol conversion efficiency. Operating at an *S/C* ratio of 1, it achieves an *r*_{H₂} of 0.034 with a heat flux of 300 W/m². Furthermore, the helical spiral design maintains acceptable CO levels, making it suitable for direct fuel cell use without requiring a purification system.

2. Modeling framework

CFD studies offer accurate findings with minimal effort compared to experimental approaches, making them particularly valuable when facing fabrication limitations. Developing an accurate model that describes the process of steam reforming in the microreactor is crucial, as the simulation aims to achieve complete conversion of methanol, maximize H₂ production rate, and minimize CO production. CFD simulations were conducted to address the current problem of the helical spiral microevaporator-microreformer coupled system, which encompasses multiphysics phenomena including laminar flow, species

Table 1

Structural details of the helical spiral microchannel evaporator-reformer design.

| Design | Parameter | Range |
|-------------------------|----------------------------|--|
| microchannel evaporator | Total length | 39.502 mm |
| | Axial length (L_{eva}) | 10 mm |
| | Hydraulic diameter | 250 μ m |
| | Total volume | 1.875×10^9 |
| microchannel reformer | Total length | 39.502 mm |
| | Axial length (L_{ref}) | 10 mm |
| | Catalyst thickness | 37.5–75 μ m |
| | Volume of catalyst | 4.782×10^8 – 7.893×10^8 μ m ³ |

transport, heat transfer, chemistry, and reaction kinetics. For this purpose, COMSOL Multiphysics 6.0 was employed, as it is a preferred finite element-based software for solving such complex multiphysics problems [25]. The numerical simulation is conducted in three main stages: (i) Preprocessing, which includes designing the microevaporator-microreformer system, selecting appropriate physics and model equations, providing material and mixture properties for the model, establishing boundary conditions, meshing, and setting solver parameters, (ii) Processing involves running the model, and (iii) post-processing entails evaluating results, plotting outcomes, and assessing species conversion and microreactor performance.

2.1. Microreactor design

The present microreactor design is unique, featuring a helical spiral-shaped microevaporator and microreformer. In this coupled system, a liquid-phase mixture of methanol and water initially enters the microevaporator, where it is heated by an external heat flux ranging from 100 to 900 W/m², transitioning the mixture from liquid to vapor phase. The spiral design of the microevaporator enables rapid mixing and vaporization of the incoming species. Once converted into a homogenized vapor mixture, the methanol and water enter the microreformer, where the methanol steam reforming reaction takes place over the catalyst coated onto the wall. This reaction leads to the production of product gas, as illustrated in Fig. 1(b). Both the microevaporator and microreformer have an axial length of 10 mm, with a pitch and diameter of 2000 μ m and 2682 μ m, respectively. Each component consists of 5 turns, as illustrated in Fig. 1(c). The microchannel diameter is 250 μ m, and also the hydraulic diameter (Fig. 1(d)). The microreformer has a wall coated catalyst of Cu/ZnO/Al₂O₃ on its inner surface. In the CFD analysis, four designs (D1–D4) were investigated, featuring microchannel inner diameters of 100, 125, 150, and 175 μ m to evaluate the influence of catalyst thickness on steam reforming performance (Fig. 1e). These designs represent a sequential reduction in catalyst thickness, with values of 75, 62.5, 50, and 37.5 μ m, respectively. The full geometric specifications of the microevaporator-microreformer coupled system are provided in Table 1.

2.2. Mathematical modeling

Solving the current coupled system requires utilizing the Multiphysics coupling feature. To depict methanol steam reforming in this coupled system, the following physics are employed: laminar flow, species transport, heat transfer in fluids, and chemistry to model interactions among different species (CH₃OH, H₂O, CO, CO₂, and H₂) while considering applied boundary conditions. The present study is based on several assumptions: steady-state conditions, laminar flow of the species, an isotropic catalyst layer with reactions occurring on its surface, isotropic thermophysical properties of the catalyst [66], and neglecting thermal radiation and gravitational effects [36]. These assumptions serve as the foundation for solving Multiphysics problems in steam reforming-based H₂ production. With the Knudsen number below 0.001, the system can be modeled using the continuum assumption, facilitating accurate application of the Navier-Stokes equation with a

no-slip boundary condition [67]. The present model encompasses continuity, momentum, energy balance, and species transport equations coupled with the reaction kinetics equations, which are solved to comprehensively analyze the steam reforming process for H₂ production [31,68].

2.3. The continuity equation

The Continuity equation represents the conservation of mass for all fluid species involved in the reaction. For the present study's weakly compressible flow case, the continuity equation can be expressed as follows [69].

$$\nabla \cdot (\rho U) = 0 \quad (1)$$

2.4. The momentum conservation equation

This equation depicts momentum conservation and is employed to ascertain the fluid velocity field [70,71]. In Eq. (2), the first term corresponds to the inertial force, the second to the pressure force, and the third to the viscous force.

$$\rho(U \cdot \nabla)U = \nabla \cdot [-PI + K] \quad (2)$$

the viscous stresses are encapsulated within the viscous stress tensor K . This tensor is defined in terms of dynamic viscosity μ (kg/ms) and velocity U (m/s) [72]. Here, I denote the unit tensor, ρ denotes density (kg/m³), and P is pressure (Pa) in the microchannel.

$$K = \mu(\nabla U + (\nabla U)^T) - \frac{2}{3}\mu(\nabla \cdot U)I \quad (3)$$

at the walls and outlet, $U = 0$, and $P = 0$.

In the present study, the microreactor incorporates a porous media layer coated onto the walls of the microreformer. A non-Darcian model is employed, since Darcy's law is valid only for Reynolds numbers (Re) < 10. Consequently, a nonlinear term is introduced using the Forchheimer equation, which includes the inertial loss coefficient (β). The diffusivity is calculated based on the binary diffusion coefficient, assuming that the gas mixture behaves as an ideal gas. In porous media, diffusivity is reduced due to the complex pathways within the structure. To account for this reduction, a tortuosity factor is introduced, calculated using the Millington and Quirk model. Furthermore, Eqs. (2) and (3) are adapted to reflect the specific setup of the microreformer, incorporating key parameters such as catalyst porosity (ϵ), permeability (κ), and β . These modifications are expressed in the form of Eqs. (4) and (5).

$$\frac{1}{\epsilon_p} \rho(U \cdot \nabla)U \frac{1}{\epsilon_p} = \nabla \cdot [-PI + K] - \left(\frac{\mu}{\kappa} + \beta \rho |U| + \frac{Q_m}{\epsilon_p^2} \right) U \quad (4)$$

$$K = \mu \frac{1}{\epsilon_p} (\nabla U + (\nabla U)^T) - \frac{2}{3} \mu \frac{1}{\epsilon_p} (\nabla \cdot U)I \quad (5)$$

Q_m is a mass source per unit volume of the porous medium

$$\nabla \cdot (\rho U) = Q_m \quad (6)$$

The energy conservation equation [73]

The conservation of energy in fluid flow encompasses heat transfer mechanisms, including convection, conduction, and internal heat generation or absorption. The local thermal equilibrium hypothesis is assumed, and for the microevaporator case, it is represented as Eq. (7).

$$\rho c_p U \cdot \nabla T - \nabla \cdot (k \nabla T) = Q \quad (7)$$

in the Eq. (7), k represents thermal conductivity of mixture (W/mK), Q denotes the heat source (W/m³), which in the present case is computed from the heat flux, and T is the temperature (K).

For the case of the microreformer, Eq. (7) can be written as:

$$\rho_f c_{p,f} U \cdot \nabla T - \nabla \cdot (k_{eff} \nabla T) = Q + Q_j \quad (8)$$

in Eq. (8), Q_j represents the heat source of reaction j and can be expressed in relation to the enthalpy of reaction H_j (J/molK) and reaction rate r_j

$$Q_j = - \sum_j r_j H_j \quad (9)$$

$$H_j = \sum_{j \in prod} v_{ij} h_j - \sum_{j \in react} (v_{ij}) h_j \quad (10)$$

at the outlet, it is assumed that convective heat transfer is dominant

$$n \cdot (-k_{eff} \nabla T) = 0 \quad (11)$$

The net energy source results from the cumulative effects of both the steam reforming and reverse water gas shift reactions, derived from the thermodynamic system utilized in the model. The effective thermal conductivity k_{eff} of the microreformer side is determined by considering the properties of the solid matrix and the mobile fluid. It is calculated using the Power Law, which determines the effective conductivity of the solid-fluid system as the weighted geometric mean of the conductivities of the solid and fluid.

$$k_{eff} = k_s^{\theta_s} \cdot k_f^{\epsilon} \cdot k_{imf}^{\theta_{imf}} + k_{disp} \quad (12)$$

where k_f is the fluid phase thermal conductivity, k_s is the thermal conductivity of the catalyst, and θ_s , and θ_{imf} represent the volume fractions of solid and immobile fluid, respectively. ϵ is the porosity, and k_{disp} is the dispersive thermal conductivity tensor.

The species conservation equation

The transport of concentrated species provides the equation for the model, which is the mass balance equation for the Maxwell-Stefan diffusion and convection equations at steady state and is presented as Eq. (13).

$$\nabla \cdot \left(\rho \omega_i U - \rho \omega_i \sum_{k=1}^n D_{e,ik} \left(\nabla x_k + (x_k - \omega_k) \frac{\nabla p}{p} \right) - D_{e,i}^T \frac{\nabla T}{T} \right) = R_i \quad (13)$$

where, $D_{e,ik}$ is the effective multicomponent Fick diffusivity for the i_k component (m^2/s), $D_{e,i}^T$ is the effective generalized thermal diffusion coefficient, ω_i is the mass fraction of species i , x_k is the molar fraction of species k ($x_k = \omega_k M_n / M_k$, $M_n = (\sum_i \omega_i / M_i)^{-1}$), R_i is the reaction rate (kg/m^3s).

At the outlet, the convective flux condition is used

$$n \cdot \left(\left(-\rho \omega_i \sum_{k=1}^n D_{e,ik} \left(\nabla x_k + (x_k - \omega_k) \frac{\nabla p}{p} \right) - D_{e,i}^T \frac{\nabla T}{T} \right) \right) = 0 \quad (14)$$

The Knudsen diffusion mechanism accounts for the interaction between gas species and the pore walls of the porous media. The effective diffusivity within the catalyst combines ordinary bulk diffusivity, based on Maxwell-Stefan diffusivities, and Knudsen diffusivity [25]. Since the reformer system involves a multicomponent gas mixture, the sum of the thermal diffusion coefficients is zero [74].

The reforming reaction is facilitated by the Cu/ZnO/Al₂O₃ catalyst. Studies [48,75], indicated that the steam reforming reaction progresses significantly faster compared to methanol decomposition and the water gas shift reaction. Therefore, the steam reforming equation (Eq. (15)) and the water gas shift reaction equation (Eq. (16)) are considered in the present study.

Complete methanol steam reforming reaction [75,76]



Water-gas shift reaction [75,76]



The reaction rate (R_{SR} and R_{rWGS}) for Eq. (15) and Eq. (16) are expressed in relation to the reaction rate constant and the molar concentration of the species as depicted in Eqs. (17) and (18)[75].

$$R_{SR} = k_1 \cdot C_{CH_3OH}^{0.6} \cdot C_{H_2O}^{0.4} \quad (17)$$

$$R_{rWGS} = k_2 \cdot C_{H_2} \cdot C_{CO_2} - k_2' \cdot C_{CO} \cdot C_{H_2O} \quad (18)$$

where k_1 and k_2 represent the forward reaction rate constants for steam reforming and the water gas shift reaction, respectively. While k_2' denotes the backward rate constant of the water gas shift reaction. The values of k_1 and k_2 can be determined using the Arrhenius equations Eqs. (19) and (20) [75], which describe the temperature dependence of rate constants.

$$k_1 = f_1 \exp(-E_1 / RT) \quad (19)$$

$$k_2 = f_2 \exp(-E_2 / RT) \quad (20)$$

where f_1 and f_2 represent the frequency factors, and E_1 and E_2 are activation energies. The rate constant k_2' is calculated using the equilibrium constant (ζ).

$$k_2' = k_2 / \zeta \quad (21)$$

In studies of steam reforming, the S/C ratio is typically chosen to be above 1 to achieve high fuel conversion. Research on steam reforming has commonly observed S/C ratios in the range of 1 to 3 [19,77,78]. This range is also selected as a key parameter to analyze its effect on methanol steam reforming. In the CFD analysis, the total mass flow rate (\dot{m}_{mix}) resulting from the mixture of methanol and water is kept constant at 10^{-5} kg/s. The \dot{m}_{mix} of the incoming streams of methanol and water are calculated using the mixing formula described in [79]. To accommodate variations in the S/C ratio, different sets of molar fractions of methanol and water are determined using Eqs. (22) and (23). These calculated mole fractions of methanol and water serve as the inlet conditions for species transport. The flow is assumed to be laminar, resulting in a $Re < 100$ for the mixture. At the inlet, there is only a liquid methanol-water mixture with a molar fraction of methanol and water ($X_{methanol}$ and X_{water}), which needs to be provided for the species transport equation and can be evaluated using the S/C ratio [30].

$$X_{methanol} = \frac{1}{1 + S/C ratio} \quad (22)$$

$$X_{water} = \frac{S/C ratio}{1 + S/C ratio} \quad (23)$$

At the inlet, a velocity boundary condition is applied based on laminar flow physics, where the velocity is computed considering the density of the mixture, which is influenced by the composition determined by the S/C ratio ($U_{in} = \dot{m}_{mix} / \rho_{mix} A_c$). At the entrance to the microchannel evaporator, the temperature of the feed is 20 °C. The outlet boundary condition is set to atmospheric pressure, and the no-slip condition is considered.

In the current simulation, the thermophysical properties of participating species in the reaction are: ρ , c_p , ratio of specific heat (γ), k , μ , and h , which are derived from the mixture's thermodynamics. In the model, two thermodynamic systems are constructed. The first system represents the mixture of methanol and water, encompassing properties for both the liquid and vapor phases of the mixture. This system facilitates obtaining coupled properties with physics, particularly for the transition of the mixture from the liquid to the vapor phase in the microevaporator. The second thermodynamic system comprises the gas system, which incorporates the thermodynamic properties of methanol, water, CO, CO₂, and H₂. For the liquid-vapor property of the mixture, the liquid

Table 2

Various parameters employed in CFD modeling of the microevaporator-microreformer system.

| Description and symbol | Value and range | Unit |
|--|---------------------|----------------------|
| Inlet Temperature (T_{in}) | 20 | °C |
| Steam to methanol ratio (S/C) [78] | 1–3 | – |
| Mass flow rate of liquid mixture (\dot{m}_{mix}) | 10^{-5} | kg/s |
| Catalyst porosity (ϵ) [81] | 0.5 | |
| Density of catalyst (ρ_s) [81] | 1300 | kg/m ³ |
| Catalyst permeability (κ) [82] | 1×10^{-16} | m ² |
| Thermal conductivity of catalyst [25] | 0.3 | W/mK |
| Gaseous constant (R) | 8.314 | J/molK |
| Frequency factor (f_1) [75] | 8×10^8 | m ³ /mols |
| Frequency factor (f_2) [75] | 4.0×10^8 | m ³ /mols |
| Activation Energy (E_1) [75] | 70,000 | J/mol |
| Activation Energy (E_2) [75] | 1.0×10^5 | J/mol |

phase is modeled using the Soave-Redlich-Kwong model, whereas the vapor phase is described using the ideal gas condition. These selected thermodynamic models are crucial for calculating thermophysical properties and considering temperature-induced changes in the mixture's thermodynamic properties during problem-solving [80]. This system is designed to couple with the reaction of species in the mixture of methanol and water vapor within the microreformer. It is instrumental in obtaining the relevant properties based on the reaction conditions.

In the initial stage of material selection for the modeling, the mixture of methanol and water with the material switch feature is applied in both the micro evaporator and micro reformer. This material switch feature aids in analyzing the transient process from liquid to vapor, particularly beneficial in the case of the microevaporator. This is where this study differs from other works. Here, the intake of species occurs in the liquid form, which subsequently transforms into the vapor phase in the evaporator, leading to complete vaporization. In the microreformer section, the vapor mixture of methanol and water undergoes conversion into useful H₂ through the steam reforming reaction over the catalyst. In contrast to other studies where researchers only simulated the micro-reformer with the species considered in the gaseous phase, here we observe the transition of the liquid methanol-water mixture to vapor. The reaction is assumed to take place exclusively in the microreformer, where the catalyst coating on the wall is applied. However, the actual scenario regarding the initiation of the reaction will be analyzed post-simulation, and the potential for reaction in the microevaporator will also be investigated. In the microreformer, a catalyst layer with wall-coating catalyst is applied, with a porosity value of 0.5. The thickness of the catalyst coating varies from 37.5 to 75 μ m, demonstrating the impact of catalyst thickness on methanol conversion performance. The parameters selected and the boundary conditions applied to solve the numerical problem of the helical spiral design are listed in Table 2.

3. Numerical method

The microreactor's current system involves a complex nonlinear relationship due to the integration of multiphysics and thermodynamics-driven material properties. Attempting to solve the entire system using a direct numerical approach encounters convergence problems. To address this issue, a segregated method for solution is adopted, which offers a more efficient approach and takes less time. The adopted approach involves obtaining the solution for the flow of species initially. Then, the transport of chemical species and heat transfer in fluids are solved, considering the initial values from the flow in the first step. Finally, the solutions are updated for flow, chemical reaction, and heat transfer in the third step [82]. This approach is well-suited for solving the present complex Multiphysics problem and effectively addresses convergence issues.

To ensure the accuracy of the numerical solution and to assess its independence from the mesh size, a grid-independent analysis was

Table 3

Grid independence study for D2 design of helical spiral microchannel evaporator-reformer at a heat flux of 500 W/m² and S/C ratio of 2.

| Number of elements | Temperature at outlet (°C) | Difference in methanol mole fraction | F_{H_2} | F_{CO_2} |
|--------------------|----------------------------|--------------------------------------|-----------|------------|
| 95,051 | 241.04 | 0.3333 | 0.59077 | 0.19663 |
| 120,774 | 241.01 | 0.3333 | 0.59050 | 0.19651 |
| 200,563 | 241.18 | 0.3333 | 0.59108 | 0.19633 |
| 345,025 | 241.02 | 0.3333 | 0.59569 | 0.19775 |
| 699,507 | 241.14 | 0.3333 | 0.59506 | 0.19743 |

conducted. This analysis aimed to determine the effect of mesh size on the simulation results obtained from the present model. A grid-independent analysis was performed under the conditions of a heat flux of 500 W/m² and a S/C ratio of 2. Key parameters such as the average surface temperature at the outlet, the difference in methanol mole fraction, and the mole fraction of H₂ and CO₂ at the outlet of design D2 were observed to assess the effect of the number of elements. This analysis aimed to select an appropriate number of elements that would yield results with minimal deviation while minimizing computational time. In the present design, D2, a total of 200,563 elements were selected. As indicated in Table 3, the deviation between the results obtained with this number of elements is below 1 %, ensuring reliable and accurate simulations. The same evaluation process was applied to the other designs, namely D1, D3, and D4. After careful assessment, the optimal number of elements was determined to be 220,041 for D1, 191,292 for D3, and 198,941 for D4. These selections were made to strike the right balance between computational efficiency and result accuracy for each design configuration. Apart from that, after creating the meshes, the quality of elements is also assessed using element skewness as a proxy for quality, which is the default measure for mesh quality in COMSOL. An overall quality of 1 is the best possible, whereas 0 represents a degenerated element. The present average quality value is not below 0.65 in all of the designs, depicting the better quality of the mesh.

In order to validate the numerical results for the coupled system, all four designs of the microreactor are tested. Fig. 2 illustrates a comparison of simulation results for all designs in the present case with the predicted values from the methanol conversion correlation (Eq. (24)) proposed by Suh et al. [81]. In Eq. (24), all parameters from the present simulation across all designs are used to evaluate the conversion of methanol and compared with the direct methanol conversion result from the simulation based on Eq. (26). In this correlation, the dimensionless term ($m_s \bar{k}_{R,0} / V_{I,0} \rho_s$) in the Eq. (24) is associated with the ratio of the characteristic time of methanol flow $m_s / F_{I,0} \rho_s$ to the time for the methanol chemical reaction in the reformer $1 / \bar{k}_{R,0}$. This relationship indicates that methanol conversion increases with an increase in the dimensionless term. Fig. 2 illustrates small discrepancies between the simulation and the data from the correlation, demonstrating that the proposed three-dimensional (3D) model adequately describes complete methanol steam reforming and can be used for further simulation studies.

$$\eta = -1.222 + 0.00061T(K) - (1.087 - 0.0033T(K)) \ln \left(\frac{m_s \bar{k}_{R,0}}{V_{I,0} \rho_s} \right) \quad (24)$$

$$\bar{k}_{R,0} = (1 - \epsilon) \rho_s k_{R,0} \quad (25)$$

$$\eta = \frac{F_{\text{methanol},in} - F_{\text{methanol},out}}{F_{\text{methanol},in}} \quad (26)$$

where, $k_{R,0}$ represents the volumetric reaction constant for reforming (m³/kgs), $\bar{k}_{R,0}$ is the modified reaction constant for reforming, ρ_s is the catalyst density (m³/kg), $V_{I,0}$ volumetric feed rate at inlet (m³/s), m_s is the mass of catalyst (kg), and F is the mole fraction.

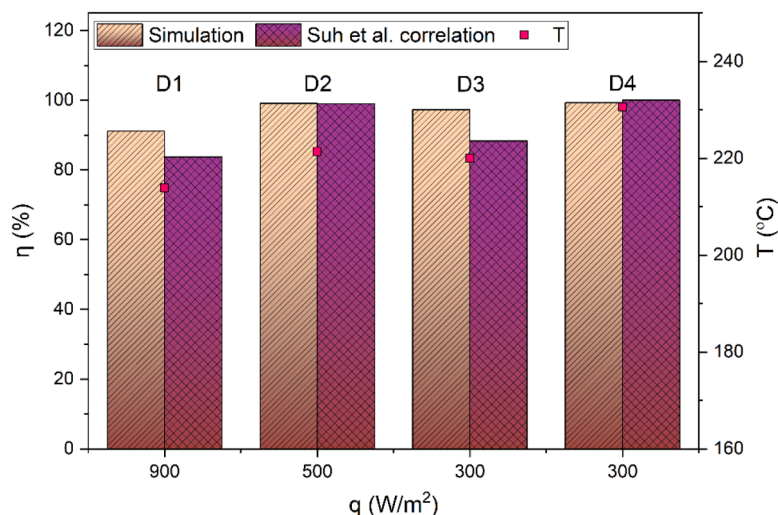


Fig. 2. Comparison of the present simulation results with the conversion performance predicted by the correlation proposed by Suh et al. [61].

4. Result and discussion

4.1. Steam reforming in the coupled system of microevaporator-microreformer system

To demonstrate the behavior of the microevaporator-microreformer system during steam reforming, we present results for a heat flux of 500 W/m² and a S/C ratio of 2. Figs. 3–6 depict the steam reforming process of the methanol-water mixture, which converts into the products of H₂, CO₂, and CO along the flow direction of the mixture for coupled system Designs D1–D4. In the figure, the constant mole fractions of water and methanol within the microevaporator indicate that no reactions occur within this component. Instead, the microevaporator results in an increase in the temperature of the mixture and subsequently, its vaporization. However, upon entry into the microreformer, the vapor mixture transforms, as evidenced by alterations in the contour of all species, indicating the onset of reactions within the microreformer as depicted in Fig. 3(a). In Fig. 3(b), the mole fraction of species along the arc length of the microreformer for the D1 design is depicted. Upon entry of the methanol-water vapor into the microreformer, an increase in the mole fraction of H₂ and CO₂ is observed, indicating rapid H₂ formation that intensifies along the flow direction of the microreformer. Conversely, the mole fraction of methanol decreases along the flow of the microreformer, suggesting a higher concentration of H₂ and CO₂ [45]. In the case of the D1 design, a methanol conversion of 60.92 % was achieved, with maximum mole fractions of H₂ and CO₂ at the outlet measuring 0.36462 and 0.11994, respectively. Conversely, significant performance improvement was observed for the D2 design under identical reaction conditions. As illustrated in Fig. 4, the D2 design facilitated complete methanol conversion (100 %) in the microreformer, with mole fractions of H₂, CO₂, and CO at the outlet recorded as 0.591, 0.1962, and 0.004795, respectively. For the D3 design, complete methanol conversion occurred in a relatively shorter length compared to the D2 design, as depicted in Fig. 5. Although there was no significant change in the values of H₂ and CO₂, a minor increment in the CO mole fraction to 0.0055 was observed.

The findings demonstrate that in the helical spiral design case, the low thickness microreformer allows for faster conversion of methanol compared to the thicker counterpart. As depicted in Fig. 6, complete conversion occurs over a relatively shorter length of 57 mm in the microreformer for the D4 design compared to the D1 design, where the entire length is insufficient for complete methanol conversion. It's noteworthy that the D2–D4 designs of the helical spiral microreformer enable complete methanol conversion while also resulting in the

formation of very small amounts of CO. In the case of the low thickness catalyst design, which facilitates higher temperatures of the mixture, an increase in temperature within the reformer leads to an increase in the CO mole fraction, aligning with findings from other studies [83].

The reason behind the lower conversion for the D1 design lies in its high catalyst thickness, which introduces thermal resistance, resulting in relatively lower temperatures within the mixture. Consequently, this leads to comparatively lower conversion rates compared to other designs. A detailed discussion on the effect of supplied heat flux is provided in the next section, where the results of a parametric study on the present design are explored. It's noteworthy that fuel and product conversion in the microreformer are interconnected with the supplied heat and the S/C ratio. Therefore, in the subsequent stage of the simulation, a parametric study is conducted to observe the effects of heat supply and S/C ratio on product formation.

The results demonstrated the steam reforming reaction for the proposed design of the helical spiral microevaporator-microreformer system. It's also recognized that in addition to design, parameters such as the supplied heat and the S/C ratio have a significant effect on the microreformer performance. To analyze the impact of these parameters, 100 simulation runs were conducted, comprising the evaluation of all four designs of the microreformer across five different heat fluxes and five S/C ratios. The results depicted in Figs. 7–10 present the species conversion to H₂, CO₂, and CO for D1, D2, D3, and D4 designs over variations in the heat flux and the S/C ratio. The effect of the heat flux and the S/C ratio leads to different rates of species conversion in the various designs, depending on the thickness of the catalyst in the microreformer. The methanol conversion performance is calculated using Eq. (26).

As depicted in Fig. 7(a), there is no change in the methanol, indicating that no reaction is taking place at the condition of heat flux = 100 W/m² in the D1 design. At this condition, the temperature of the mixture is not sufficient to trigger the reaction, with the temperature at the reformer inlet below 55 °C. Even with the increased length, the temperature of the mixture increases to reach a value of 97 °C, but this amount of temperature is not sufficient for conversion. Hence, there is no conversion of species into the product. With the increased heat flux value to 300 W/m², a small change in species is observed in the D1 design. At this heat flux, the mixture reformer outlet temperature reaches 147.35–163.18 °C for S/C = 1 and 3, respectively. At this point, a small amount of H₂ mole fraction can be seen at the microreformer outlet, varying between 0.0055–0.10164 for S/C = 1–3. Additionally, CO₂ is observed in small amounts, while the CO mole fraction remains zero, as shown in Fig. 7(b). As illustrated in Fig. 7(c), for heat flux = 500 W/m², there is an increase in the conversion of methanol and species

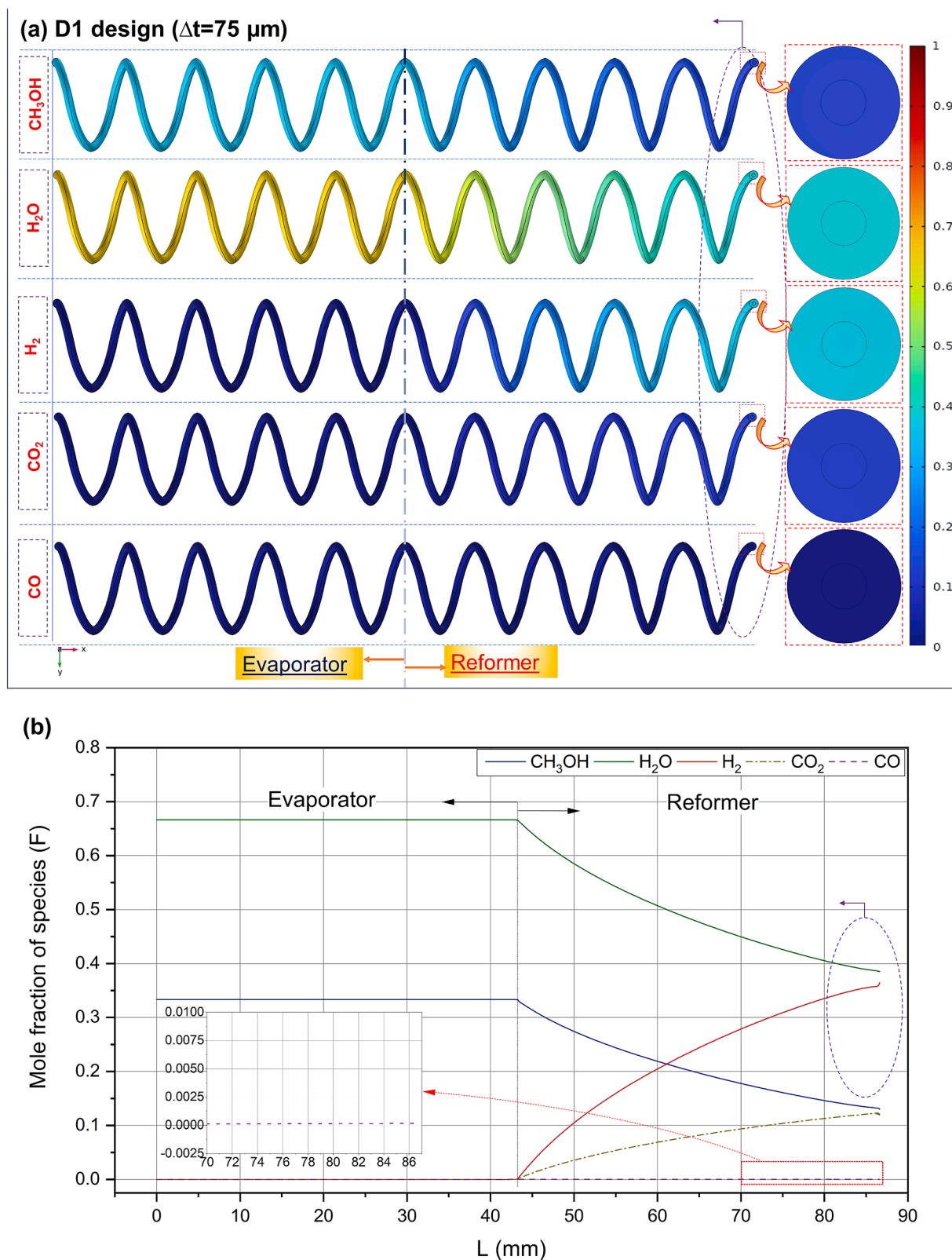


Fig. 3. (a) Contours of fuel conversion in the microevaporator-microreformer coupled system at a heat flux of $500\ \text{W/m}^2$ and an S/C ratio of 2, (b) Mole fraction of species along the arc length of the microreactor for the D1 design.

conversion observed. In this case, the temperature at the microreformer inlet and outlet varies between $157.61\text{--}187.91\ ^\circ\text{C}$ and $181.86\text{--}202.86\ ^\circ\text{C}$, respectively, for $S/C = 1\text{--}3$. This temperature is significantly high, leading to the conversion of methanol from 38.56% - 78.65% for S/C

ratios of $1\text{--}3$. Additionally, H_2 and CO_2 are observed to increase along the length of the microreformer. At the outlet of the microreformer, the mole fraction of H_2 varies between $0.2881\text{--}0.3928$ for S/C ratios of $1\text{--}3$, while the CO_2 mole fraction remains below 0.13 , and there is a

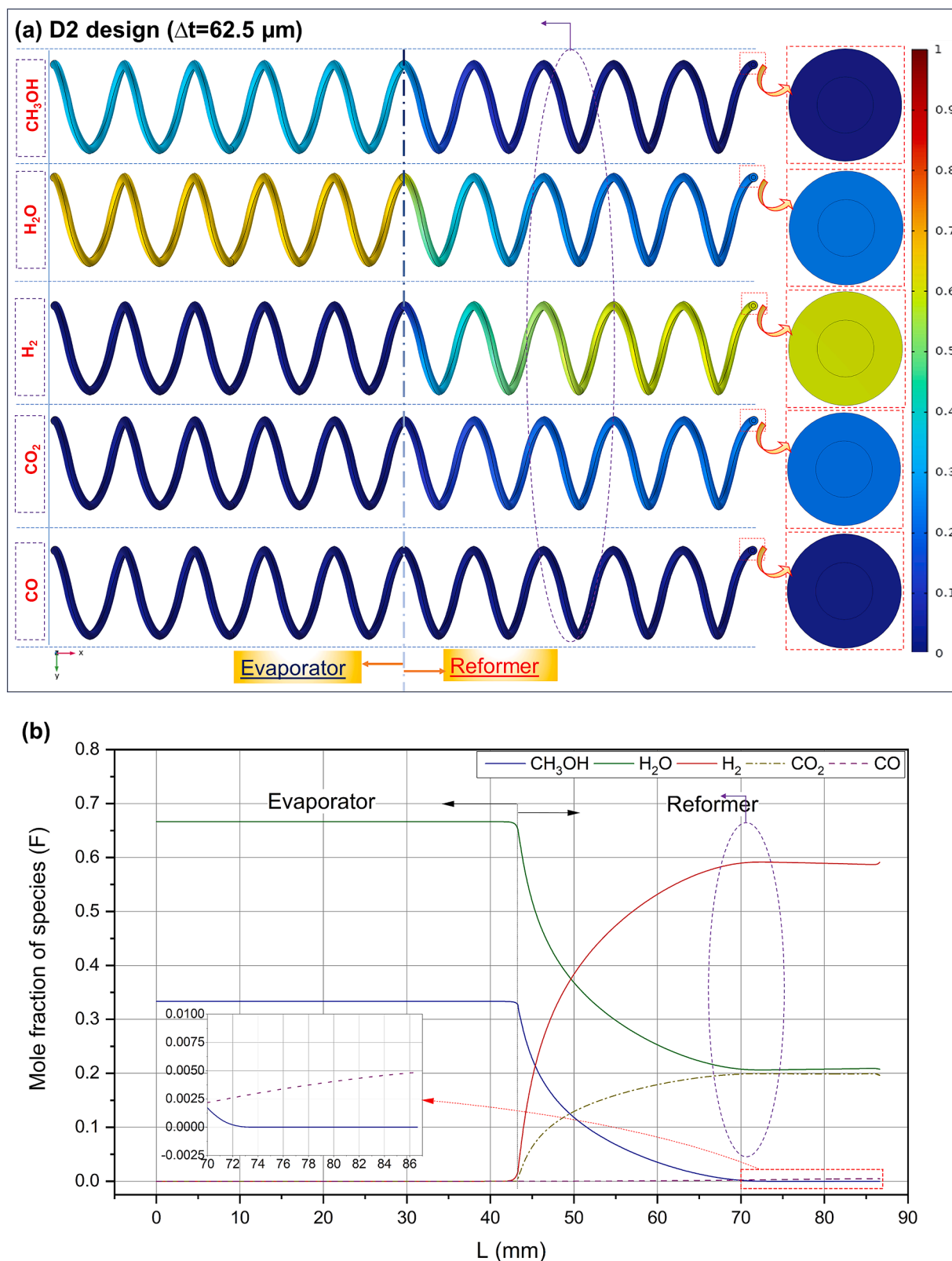


Fig. 4. (a) Contours of fuel conversion in the microevaporator-microreformer coupled system at a heat flux of 500 W/m^2 and an S/C ratio of 2, (b) Mole fraction of species along the arc length of the microreactor for the D2 design.

negligible amount of CO.

With a further increase in the heat flux to 700 W/m^2 , the mixture temperature at the inlet of the microreformer increases to $205.96\text{--}233.46^\circ\text{C}$, while at the outlet, the mixture temperature

increases to $210.51\text{--}241.44^\circ\text{C}$. This leads to the conversion of methanol from 73.1 % to 100 % for S/C ratios of 1–3, as depicted in Fig. 7(d). Additionally, a significant increase in the H_2 mole fraction is observed for this case of the supplied heat flux, ranging between 0.5494–0.4946.

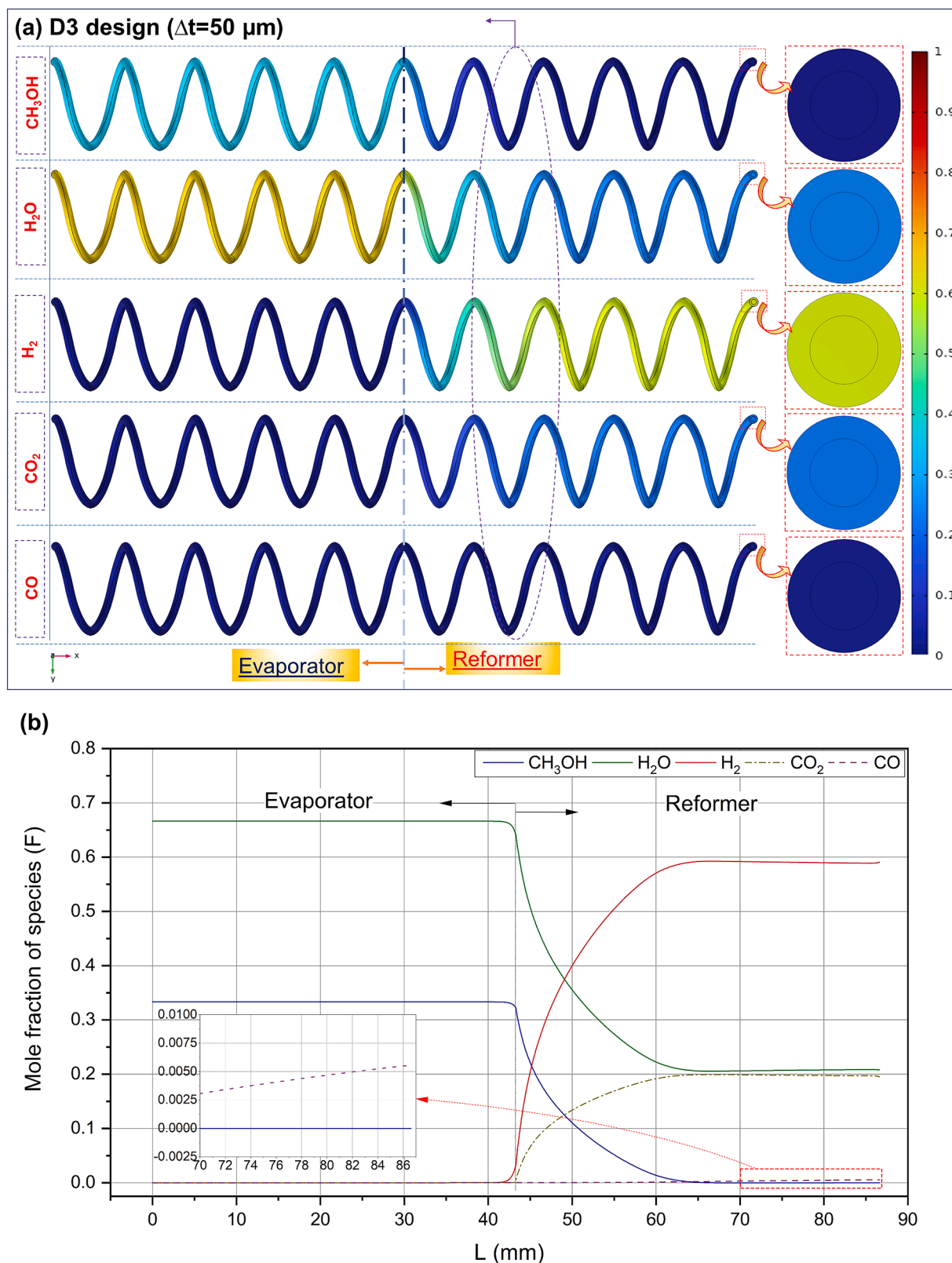


Fig. 5. (a) Contours of fuel conversion in the microevaporator-microreformer coupled system at a heat flux of 500 W/m^2 and an S/C ratio of 2, (b) Mole fraction of species along the arc length of the microreactor for the D3 design.

The CO_2 mole fraction also increases, ranging between 0.1801–0.1619 for the case of $S/C = 1$ –3. The mole fraction of CO reaches 0.0035. It's worth noting that in Fig. 7(a–c), high S/C ratios favor an increase in H_2 production for the D1 design. However, for a heat flux of 700 W/m^2 , an

increase in the S/C ratio leads to a decrease in H_2 production, while the same effect of increased conversion is observed in all cases of the supplied heat flux with an increase in the S/C ratio. A similar effect is also observed for the case of the heat flux supply of 900 W/m^2 . With the

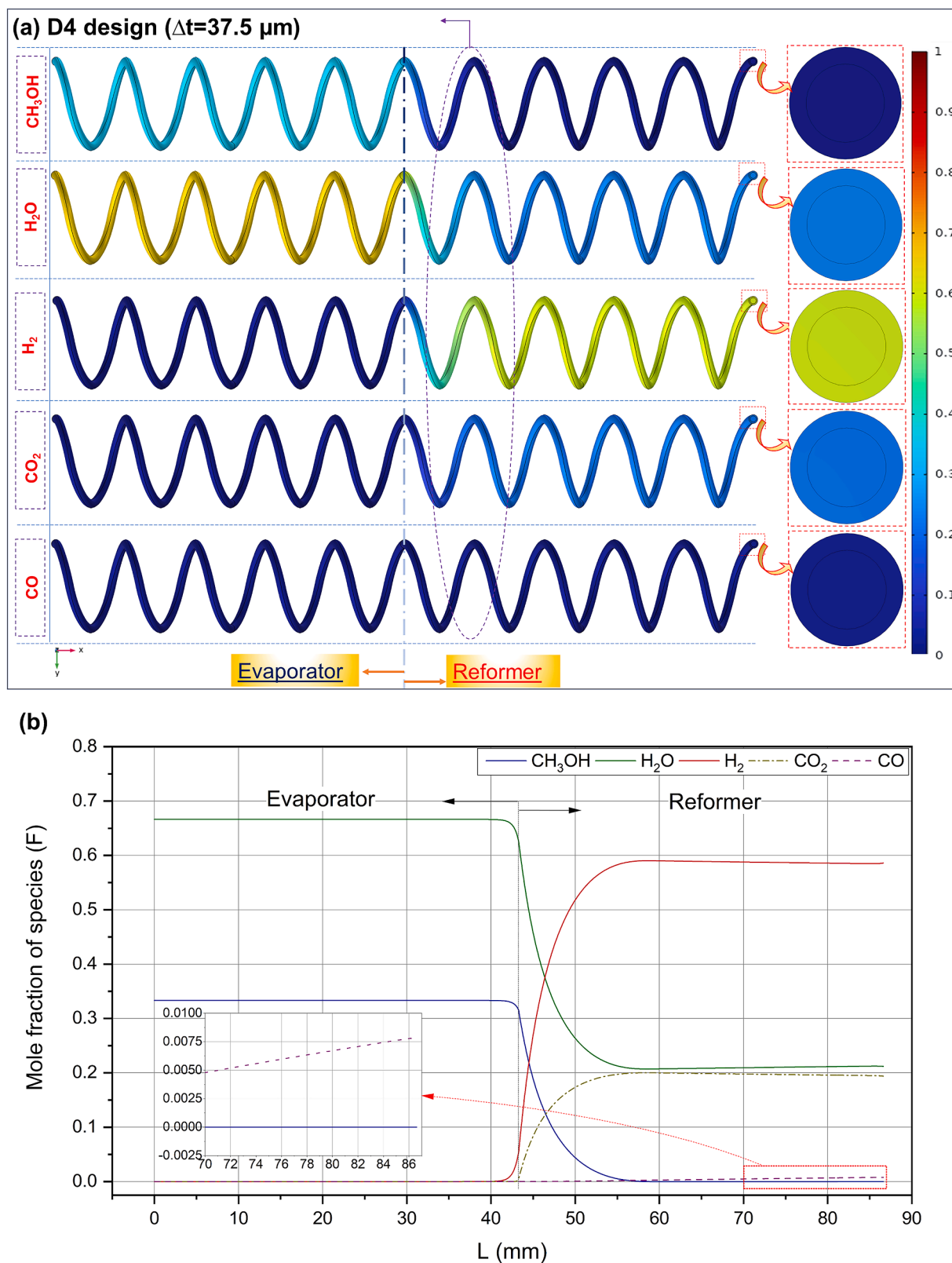


Fig. 6. (a) Contours of fuel conversion in the microevaporator-microreformer coupled system at a heat flux of 500 W/m^2 and an S/C ratio of 2, (b) Mole fraction of species along the arc length of the microreactor for the D4 design.

further increase in the heat flux, the temperature rises from 232.79 to $246.02 \text{ }^\circ\text{C}$ at the microreformer inlet, while at the outlet, it ranges from 238.86 to $265.24 \text{ }^\circ\text{C}$.

As depicted in Fig. 7(e), there is a decrease in the H_2 mole fraction for

higher S/C ratios, with the value varying between 0.683 – 0.48 for S/C ratios of 1 – 3 . Meanwhile, the CO_2 mole fraction varies between 0.2230 – 0.1575 for S/C ratios of 1 – 3 . The high thickness catalyst design shows that an increase in the heat flux leads to enhanced H_2 production.

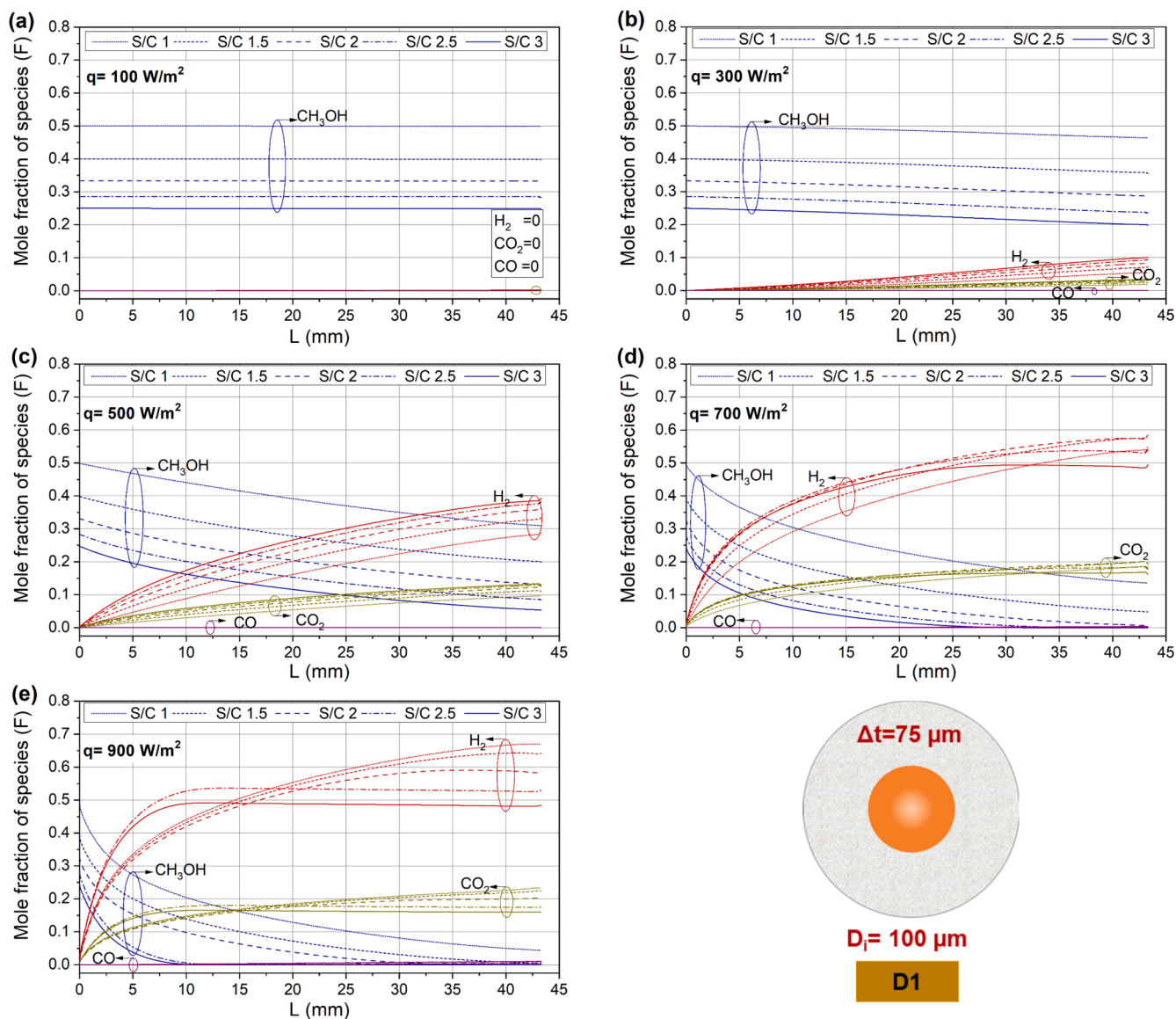


Fig. 7. Conversion of species products along the arc length in the microreformer for the D1 microreformer.

Since the reforming reaction is endothermic, increasing the heat flux results in higher temperatures, leading to more H_2 production due to increased methanol conversion for this design. For designs D2 to D4, a similar trend in species conversion is observed, as depicted in Figs. 8–10. The notable difference lies in the fact that reducing the thickness of the helical spiral microreformer catalyst enables complete conversion over a shorter length span. Higher S/C ratios facilitate quicker conversion compared to lower values, although it's observed that higher S/C ratios tend to reduce the H_2 mole fraction. For the D2 design, the temperature at the inlet and outlet of the microreformer varies between 75.51 °C and 240.01 °C, and 129.24 °C and 247 °C, respectively, with increasing heat flux from 100 to 900 W/m². This temperature variation correlates with methanol conversion rates ranging from 1.84 % to 100 %, as shown in Fig. 8. Higher heat flux and S/C ratios promote methanol conversion. The highest mole fraction observed for H_2 in D2 is recorded at 0.7356 for a heat flux value of 900 W/m², as depicted in Fig. 8(e).

In the D2 design, complete methanol conversion occurs within just 16.775 mm of microreformer length at a heat flux of 900 W/m². The increase in heat flux also results in a slight increment in CO; for the D2 design, the maximum mole fraction observed at 900 W/m² was 0.009341 at S/C = 1. In the case of the D3 design, the maximum

temperature at the outlet of the reformer reached 251.73 °C. D3 design achieves complete methanol conversion for heat flux ranging from 300 to 900 W/m², as shown in Fig. 9(b–e), while for a heat flux of 100 W/m², only a minor species conversion of 22 % occurs for S/C = 3, as depicted in Fig. 9(a). The maximum molar fraction of H_2 observed was 0.73369 for S/C = 1 and heat flux = 700 W/m². In the case of the D4 design, which has a minimum thickness of 37.5 μm, complete methanol conversion occurs in <10 mm of length in the microreformer, as depicted in Fig. 10(e). For the D4 design, the inlet temperature of the microreformer varies between 118.35–247.6 °C, and at the outlet, it varies between 165.18–256.57 °C for heat flux ranging from 100 to 900 W/m². The maximum mole fraction appears as 0.735 in the case of 700 W/m². It's worth noting that while high heat fluxes are suitable for fast conversion, they also cause a small reduction in H_2 and a minor increment in CO.

To comprehensively analyze the performance of the different designs of the microreformer and reduce the data for a comprehensive comparison, this analysis focused on two cases: (i) S/C = 2 and heat flux variation (Fig. 11(a, c and e)) and (ii) heat flux=500 W/m² and S/C variation (Fig. 11(b, d and f)). For comparing the performance of different designs of the microreformer, the outlet temperature of the microreformer, r_{H_2} , and CO mole fraction were analyzed in these two

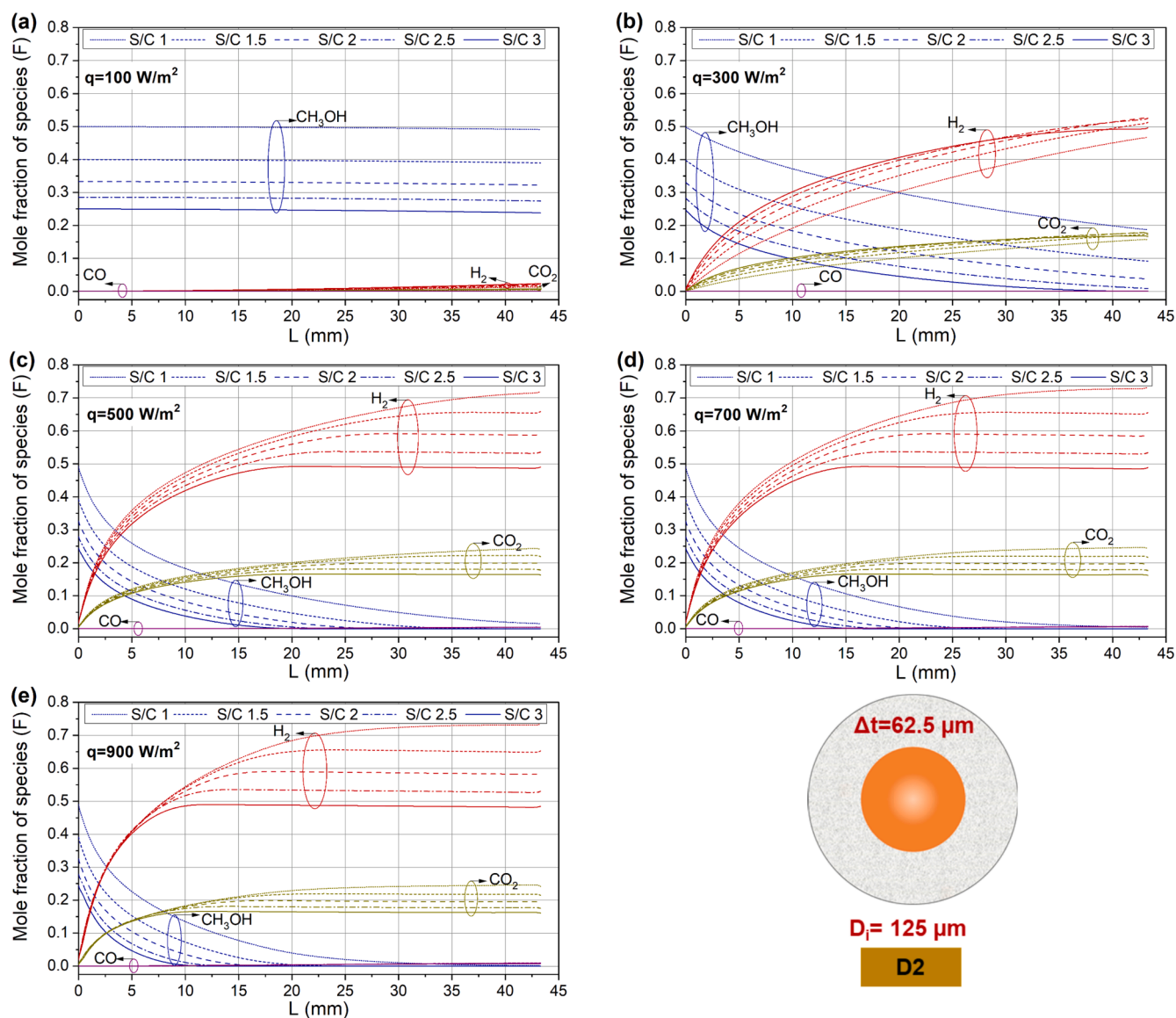


Fig. 8. Conversion of species products along the arc length in the microreformer for the D2 microreactor.

cases. In most instances, fuel conversion reaches 100 %, albeit at varying rates among different designs. This section presents qualitative results. The H_2 production rate (r_{H_2}) can be expressed by Eq. (27) in terms of the ratio of the molar flow rate of H_2 (\dot{n}_{H_2}) (mol/min) per unit weight of catalyst (g.cat) [84]. This parameter is crucial for accounting for the catalyst effect on H_2 production using the microreactor.

$$r_{H_2} = \frac{\dot{n}_{H_2}}{\text{weight of catalyst}} \quad (27)$$

The analysis of temperature directly relates to microreactor performance. The surface temperature at the outlet of the microreformer is presented in Fig. 11(a and b). Fig. 11(a) indicates that the increase in the heat flux results in an increase in the outlet temperature of the species products from the microreformer. In the case of $S/C = 2$ and a heat flux of 100 W/m^2 , the temperature at the outlet of the D1-D4 designs varied between 93.141°C to 173.03°C . This indicates that the design D1 with high catalyst thickness does not achieve a sufficient temperature at 100 W/m^2 , consequently resulting in no reaction. Conversely, the low thickness design allows higher temperatures to be reached in the mixture, facilitating faster conversion of species due to its lower thermal resistance compared to the high catalyst thickness design. It's worth

noting that when the fluid mixture achieves a temperature of approximately 240°C , further increases in heat flux do not result in a significant temperature rise. However, a slight increase in CO concentration is observed when the temperature exceeds the optimal condition, as shown in Figs. 8–10 for a supplied heat flux of 900 W/m^2 . From Fig. 11(b), it is evident that at a heat flux of 500 W/m^2 , increasing the S/C ratio does not notably enhance the temperature, as the mixture has already reached the suitable temperature of 240°C for methanol steam reforming in D2-D4 designs. However, in this case of the supplied heat flux, the outlet mixture temperature of the D1 design increases from 181.7 to 202.73°C .

From Fig. 11(c), it's evident that the r_{H_2} improves with the increase in the heat flux values for the D1 design, while for the D2-D4 designs, it first increases, then it becomes almost constant. The sharp increase in r_{H_2} is observed for the D1 design, which has the highest thickness and achieves the highest r_{H_2} value of 0.054 . Conversely, the reduction in thickness results in a decrease in the r_{H_2} value. This trend of increased H_2 production with catalyst thickness is consistent with findings in the work Ref. [25]. For the other designs D2, D3, and D4, the maximum values of r_{H_2} were 0.031 , 0.025 , and 0.026 respectively. An interesting observation is made when the change in the S/C ratio leads to significant variation in r_{H_2} . The increase in the S/C ratio for the second case of

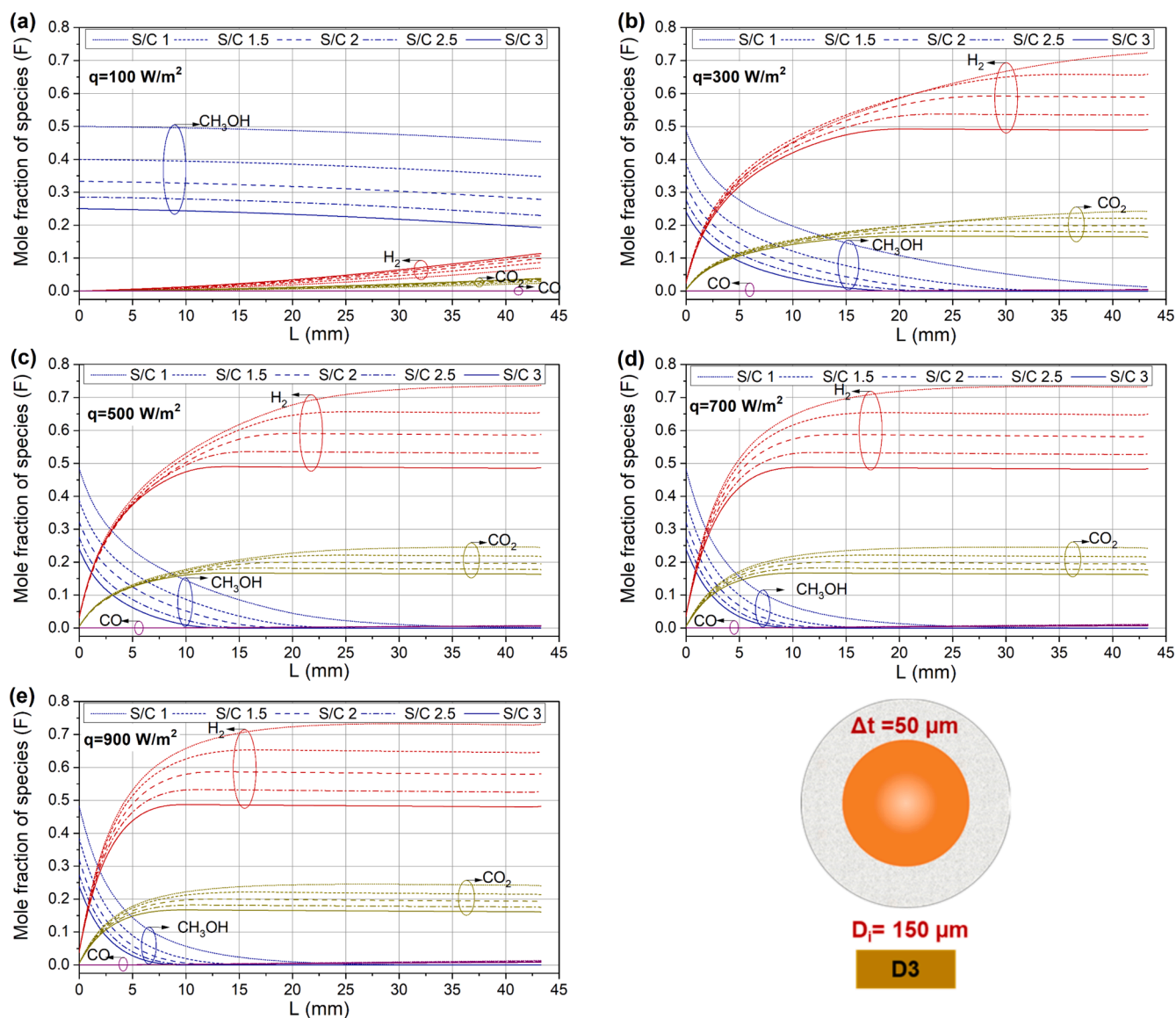


Fig. 9. Conversion of species products along the arc length in the microreformer for the D3 microreactor.

analysis results in a reduction in the r_{H_2} value, as depicted in Fig. 11(d) for D2-D4 designs. Conversely, the D1 design, which has the highest value of r_{H_2} at 0.037, a smaller increment in r_{H_2} is observed with the increase in the S/C ratio. Fig. 11(e and f) demonstrates the mole fraction variation of CO with varying heat flux and S/C ratio conditions. It's noteworthy that only a minimal amount of CO is produced in the helical design microreactor. Compared to other designs, the D1 design exhibits the lowest CO production, indicating that the high thickness catalyst configuration produces less CO compared to the low thickness configuration. This is attributed to the relatively lower temperature in the microreactor for the high thickness catalyst configuration, as shown in Fig. 11(e). With an increase in the heat flux value, a small increment in CO is observed in all designs. Conversely, an increase in the S/C ratio leads to a decrement in CO, as depicted in Fig. 11(f), because of the increment in methanol conversion with the increase in the S/C ratio. Another possible explanation for the reduction in CO is a decrease in CO formation within the CO formation zone, as evidenced by the work of Pashchenko and Makarov [85].

Fig. 12(a) illustrates the pressure changes across the microchannel for various designs. As shown in Fig. 12(b), the D1 design experiences a higher pressure drop due to its thicker catalyst layer, which narrows the

flow passages in the microreactor, restricting fluid movement. In contrast, Designs D2 through D4, with thinner catalyst layers, exhibit lower pressure drops, with D4 showing the smallest drop due to its minimal thickness. Throughout the evaluation, the total mixture flow rate (\dot{m}_{mix}) remains constant at 10^{-5} kg/s. However, variations in the S/C ratio alter the mixture composition, with a higher S/C ratio increasing the proportion of water. The D1 design shows a pressure drop ranging from 347.85 to 373.73 kPa for S/C ratios of 3 to 1, respectively. As the S/C ratio increases, the pressure drop decreases, primarily due to the higher water content, which facilitates faster conversion and gaseous product formation, reducing the pressure required to move the mixture. A similar trend is observed for the other designs, though they exhibit lower pressure drops compared to D1.

Fig. 12(c) shows velocity variations within the coupled microevaporator-microreformer system. The velocity increases along the flow path, corresponding to the pressure drop. A significant change in velocity occurs when the mixture enters the microreactor, leading to a sudden drop in pressure. This increase is more pronounced in the confined spaces of the microreactor. The velocity in the catalyst-coated region is considerably lower due to resistance caused by the high internal surface area of the catalyst, while the internal domains without

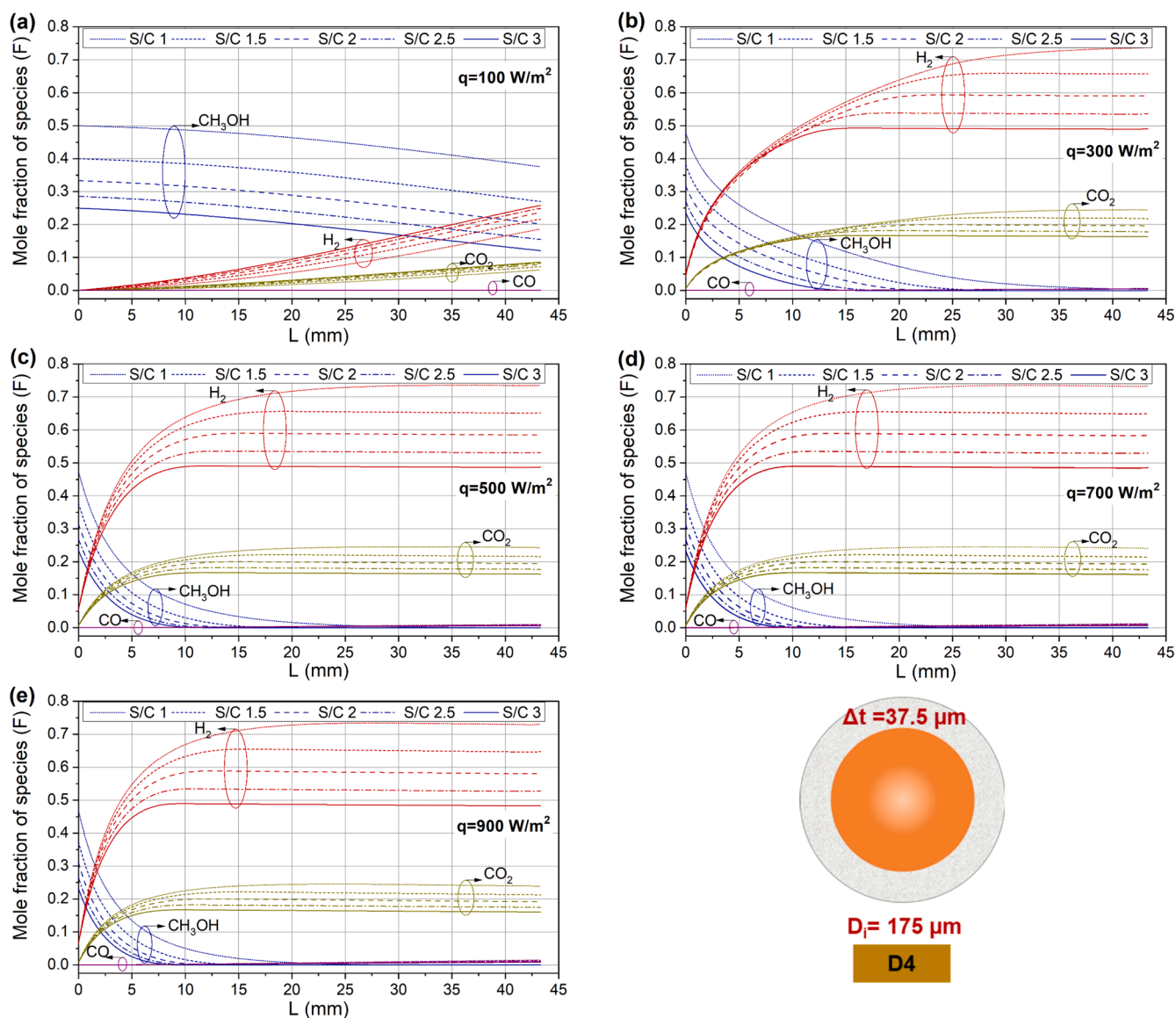


Fig. 10. Conversion of species products along the arc length in the microreformer for the D4 microreactor.

flow resistance experience a noticeable velocity increase.

4.2. Influence of different parameters in methanol steam reforming

The performance of the microreactor for H_2 production is influenced by several factors, with design being a crucial one. Additionally, reaction conditions such as supplied heat flux, catalyst thickness, and the S/C ratio also significantly affect the microreactor's performance. In this section, we will critically examine these factors and their impact on the microreactor's performance.

4.2.1. Effect of catalyst thickness

The thickness of the catalyst plays a critical role in the steam reforming process, necessitating an optimized thickness to achieve high microreactor performance. In the helical spiral microevaporator-microreformer coupled system designed in this study, a thinner catalyst layer resulted in complete methanol conversion over a shorter channel length. This outcome is attributed to several factors: the larger space within the channel facilitating improved fluid movement, the spiral channel geometry promoting better mixing, and the shorter diffusion pathways enabling efficient mass transfer of reactants to the

active sites compared to thicker catalyst layers.

However, as shown in Fig. 11(c) and 11(d), the r_{H_2} was higher for the thicker catalyst. This is due to the larger amount of catalytic material, which provides more active sites for the reaction. Achieving optimal reforming temperatures with the thicker catalyst requires a higher heat flux, as the increased heat flux helps overcome thermal gradients across the catalyst thickness. Despite these advantages, thicker catalysts exhibited relatively lower methanol conversion rates, primarily due to mass transfer limitations [86], as the diffusion of reactants to active sites becomes hindered in thicker layers. Temperature analysis further revealed that high-thickness catalyst designs experienced lower temperatures overall, owing to the thermal resistance of the catalyst. Nonetheless, a notable benefit of the thicker catalyst was its relatively lower CO production compared to the thinner catalyst design.

4.2.2. Effect of heat supply

The supplied heat flux plays a critical role in both the reforming process of the microreformer and the rapid vaporization of the methanol-water mixture in the microevaporator. To illustrate its impact, a contour plot of the temperature distribution for the D1 design is shown in Fig. 13(a). As the heat flux increases, the temperature rises along the

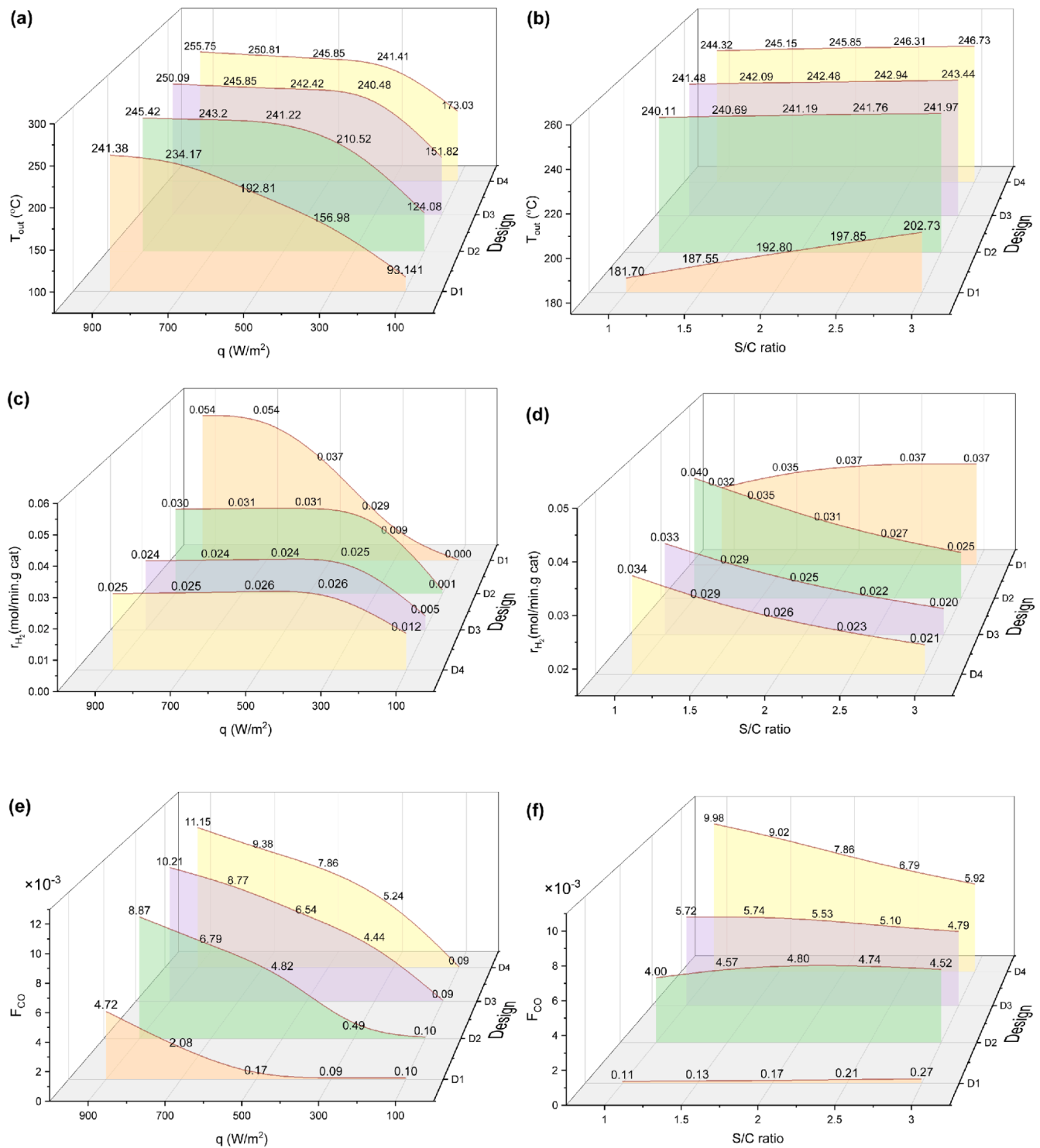


Fig. 11. (a)-(b) Effect of supplied heat flux and S/C ratio on the outlet temperature of the reformer, (c)-(d) Variation in H_2 production rate with supplied heat flux and S/C ratio, (e)-(f) Mole fraction of CO influenced by supplied heat flux and S/C ratio.

species flow path, as evident in the plot. At a high heat flux of 900 W/m², the microreformer reaches a sufficient temperature, enabling complete methanol conversion compared to lower heat flux cases. Fig. 13(b) highlights the effect of heat flux on the outlet temperature and methanol conversion for the case of S/C = 2. At a low heat flux of 100 W/m², both methanol conversion and the average outlet temperature are significantly low. However, these values increase rapidly with higher heat flux, achieving complete methanol conversion at 900 W/m². The observed trends in methanol conversion and temperature variation for the D1

design are consistent with previous findings [25]. It is noteworthy that changes in heat flux have a more prominent impact than variations in the S/C ratio, as depicted in Fig. 13(c), which shows the effect of S/C ratio variation at a constant heat flux of 500 W/m². This observation aligns with findings reported in Ref [36].

While higher temperatures improve fuel conversion, increasing the heat flux beyond 500 W/m² does not significantly enhance H_2 production for designs D2-D4. Instead, it results in elevated temperatures and slight increments in CO formation. Methanol conversion increases

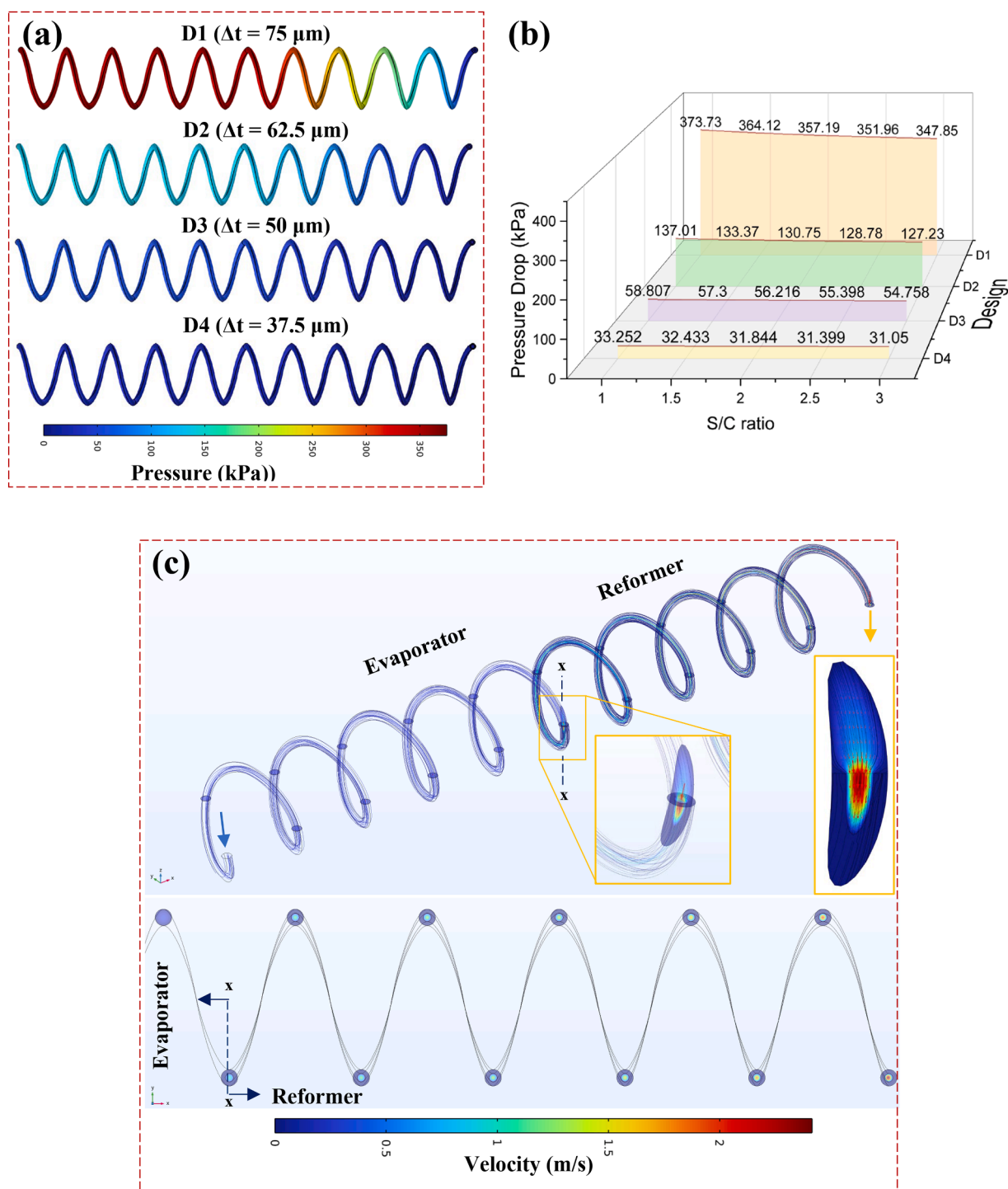


Fig. 12. (a) Pressure contours for all designs at 500 W/m² and S/C = 2, (b) Pressure drop across all designs with varying S/C ratios at 500 W/m², (c) Velocity variation in the D2 design as flow enters the reformer.

rapidly at temperatures above 230 °C and an S/C ratio of 3, after which it stabilizes. Beyond this optimal point, H₂ production does not improve and may slightly decrease due to reduced catalytic activity and the presence of CO. Figs. 7–10 illustrate that methanol conversion is strongly influenced by higher temperatures and the S/C ratio. To provide a comprehensive view of these parameters, Fig. 13(d) depicts the combined effects of heat flux and S/C ratio variations on temperature, methanol conversion, H₂ production, and catalytic activity.

4.2.3. Effect of S/C ratio

The S/C ratio significantly influences methanol conversion, but it has been observed that it does not have a substantial effect on H₂ production. An increase in the S/C ratio reduces CO formation, as directly observed in the case of the D1 design in Fig. 11(f), and also slightly increases the temperature, as shown in Fig. 13(c). Additionally, a higher S/C ratio facilitates faster methanol conversion, but the H₂ mole fraction decreases. This trend is consistent with the findings of Hafeez et al. [25].

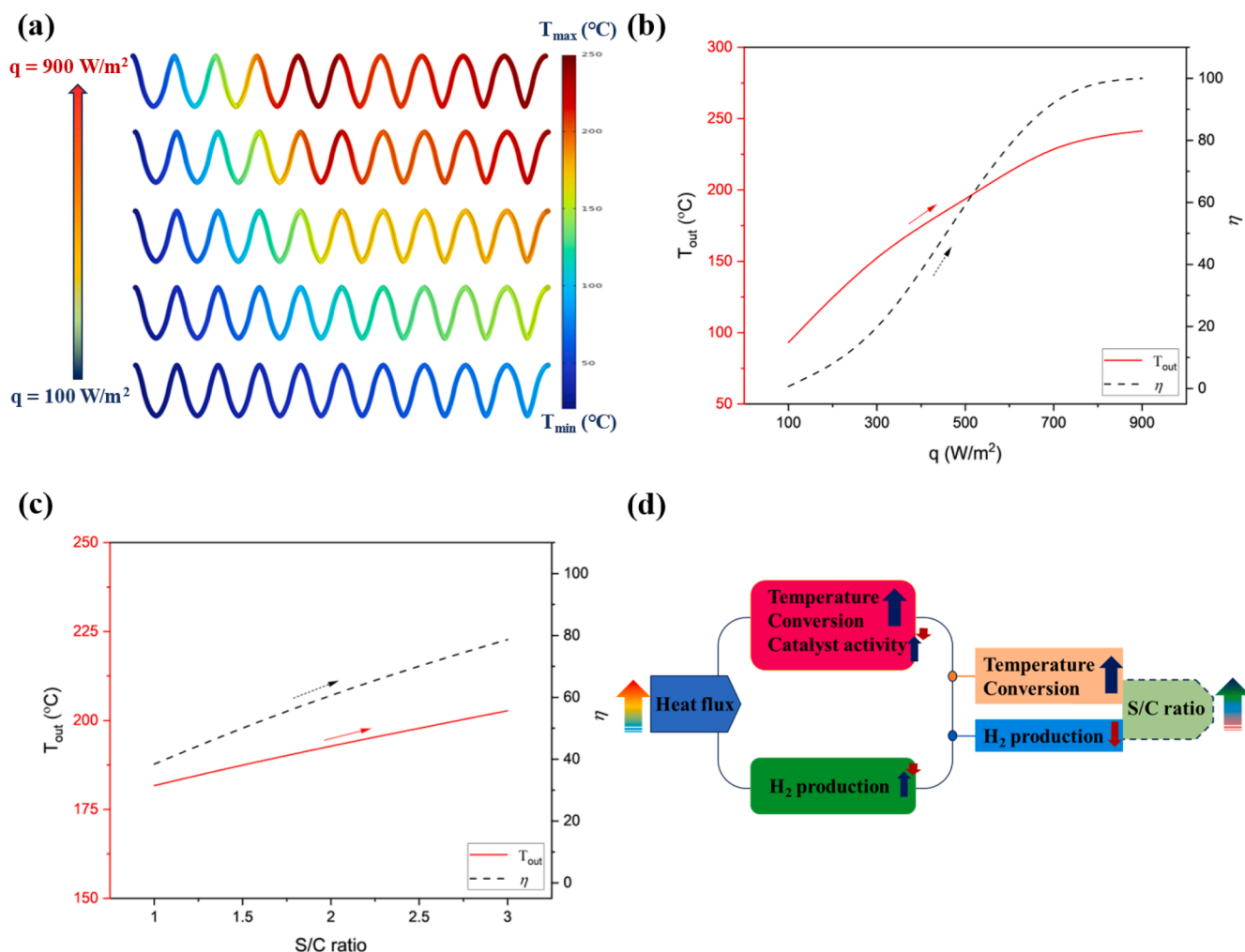


Fig. 13. Influence of heat flux and S/C ratio on the performance of the helical spiral microreactor: (a) Contour plot showing the impact of heat flux on temperature distribution in the microevaporator-microreformer coupled system, (b) Effect of heat flux on methanol conversion and outlet temperature, (c) Effect of S/C ratio on methanol conversion and outlet temperature, and (d) Illustration of the combined effect of heat flux and S/C ratio.

4.2.4. Effect of reactor length

It's worth noting that the length of the microchannel has a significant impact on the performance of the microreactor. A larger length is beneficial for handling a larger volume, as it increases the surface area and provides more time for the reaction to occur [87]. Although the total length for both the microevaporator and microreformer was the same in all designs, surprisingly, each design enables complete conversion over different lengths. The design with the small thickness catalyst, the D4 design, showed the fastest conversion compared to other designs, with complete conversion occurring in just 1/5th the length of the microreformer. In contrast, the high thickness catalyst D1 design takes the whole length for conversion. The completion of the conversion is also directly linked with the combination of the supplied heat flux and the S/C ratio of the mixture.

The behavior of the coupled system and its variation in species conversion can be understood by analyzing the temperature of the mixture, which is directly influenced by the supplied heat, S/C ratio, and catalyst thickness. Fig. 14 depicts the temperature variation of the mixture along the arc length of the microevaporator-microreformer coupled system. In the numerical problem formulation, it was initially assumed that the microevaporator only facilitates the vaporization of the mixture. Subsequently, this vaporized mixture undergoes reactions over the catalyst surface in the microreformer. Interestingly, both channels are interconnected, and since there is no reaction occurring in

the microevaporator, the mixture temperature should theoretically continue to rise. However, because steam reforming is an endothermic process, the mixture entering the microreformer is expected to undergo a temperature decrease. Therefore, it becomes intriguing to examine how the combination of supplied heat and the S/C ratio will affect steam reforming in the different designs.

For the depiction of this behavior, the results have been shown for the two different cases. In the first case, depicted in Fig. 14(a–d), the supplied heat flux is maintained at 500 W/m^2 in all designs, while the S/C ratio varies. In the second case, the results are presented for an S/C ratio of 2, while the heat flux varies between 100 and 900 W/m^2 , as depicted in Fig. 14(e–h). As depicted in Fig. 14, steam reforming occurs within the microreformer, consuming the energy provided by the externally supplied heat flux. Consequently, the temperature of the methanol-water mixture entering the microreformer experiences a sudden drop. As the feed progresses in the flow direction inside the channel, it begins to convert into the product, leading to an increase in temperature. An important observation is that the response behavior of different individual designs remains consistent for the same applied heat flux and variations in the S/C ratio. Although the S/C ratio significantly improves conversion, the species conversion behavior remains consistent, as also observed in Figs. 8–10. The concept of heat absorption and the behavior of reactions striving to attain thermal equilibrium conditions can be grasped by examining the temperature graph of the

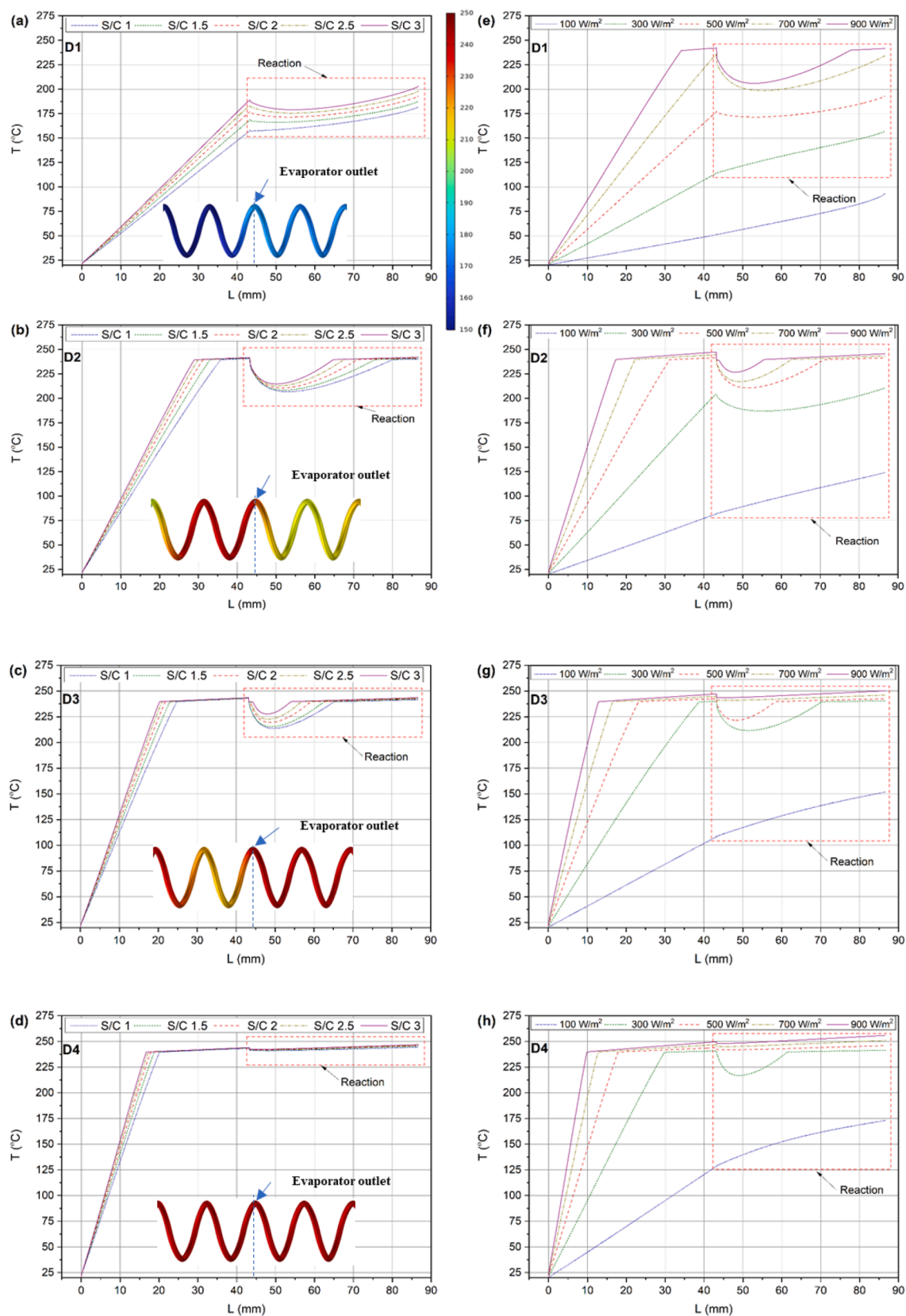


Fig. 14. Temperature variation of the mixture along the arc length of the microreactor for different designs:(a)-(d) at a heat flux of 500 W/m², (e)-(h) at an S/C ratio of 2.

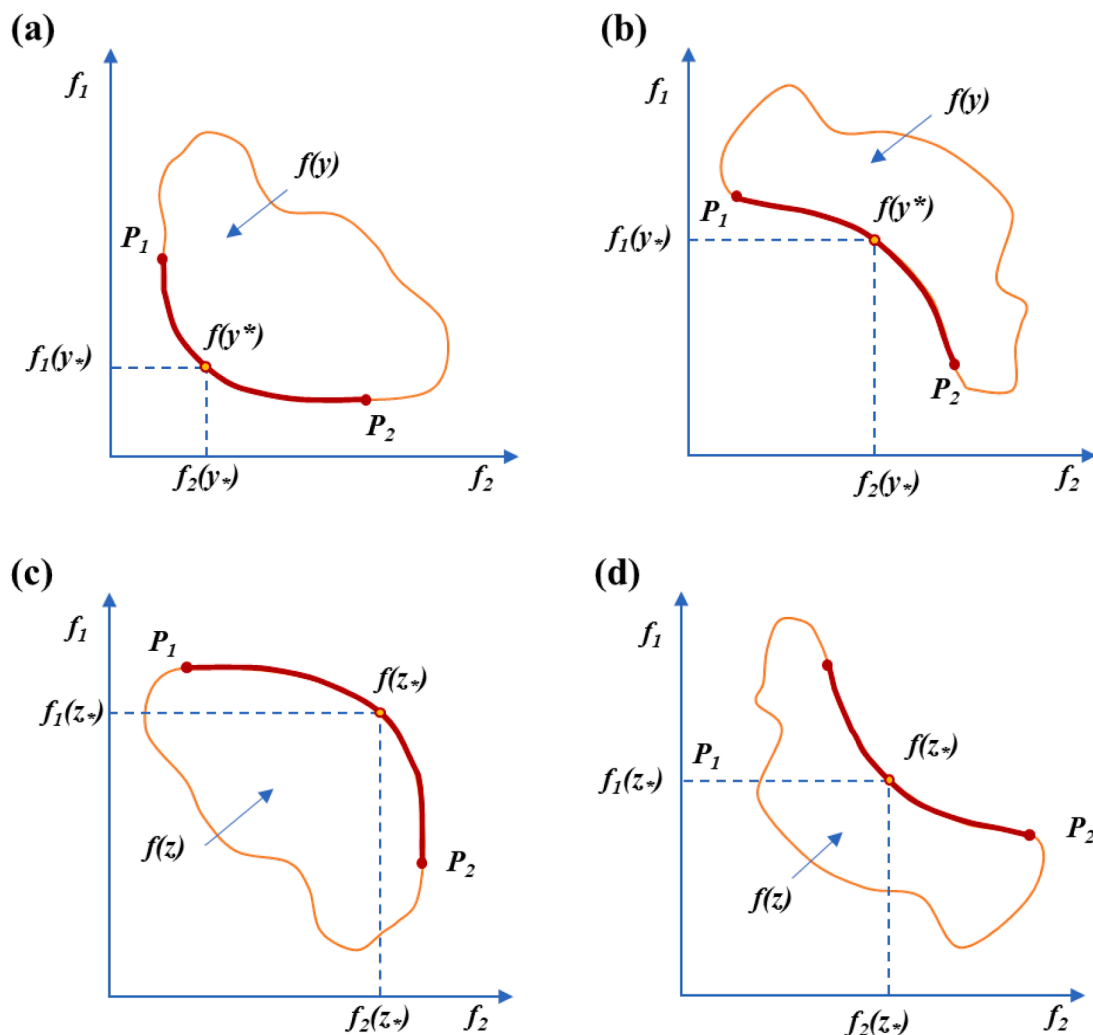


Fig. 15. Pareto fronts for two-objective optimization: Minimization case — (a) Convex, (b) Nonconvex; Maximization case — (c) Convex, (d) Nonconvex.

microreactor, as illustrated in Fig. 14(a–d) for the case of heat flux = 500 W/m² and $S/C = 2$. It was also observed that for microreformer designs with lower thickness catalysts and at high heat flux, the species begin reacting before entering the microreactor. This is evident from the decrease in temperature contour shown in Fig. 14(a–c), indicating heat absorption for the reaction. Catalysts with higher thicknesses exhibit a larger span of reduced temperature, indicating a slower conversion process (Fig. 14(a)). A thinner catalyst thickness allows for quicker heat transfer and significantly enhances the temperature of the mixture due to the relatively higher temperature at the catalyst wall resulting from lower thermal resistance. This is the reason that the area of the temperature drop reduces with the thickness of the catalyst, which also correlates with faster conversion of methanol, as shown in Fig. 14(b–d). In the case where the mixture temperature is below 175 °C, only a small conversion is observed. However, when the temperature reaches between 225 and 250 °C, it favors methanol steam reforming. Within this temperature range, the reaction tends to approach thermal equilibrium, indicating a clear balance of energy where the supplied heat is directly utilized in fuel conversion, resulting in no significant change in temperature (Fig. 14(d)). From Fig. 14(a–d), it's visible that in the high thickness catalyst design D1, the mixture has the lowest temperature at the outlet of the microevaporator and microreformer compared to the low thickness design. The maximum temperatures reported at the outlet of the microreformer for D1, D2, D3, and D4 for the first case were ~203 °C, ~242 °C, ~244 °C, and ~247 °C, respectively.

In contrast, for the second case where the supplied heat varies for the

designs while maintaining the same S/C ratio, it becomes evident that the supplied heat flux has a more significant impact on steam reforming compared to the S/C ratio. The variation in the supplied heat flux leads to a substantial change in the temperature of the mixture, as illustrated in Fig. 14(e–h). Higher heat flux values facilitate the rapid vaporization of the mixture. A temperature range of 225–250 °C is observed, indicating a state where the fluid mixture vapor attempts to maintain an isothermal condition. Mixtures entering the microreformer below this range experience a sharp decrease in temperature, signifying heat absorption. When the mixture enters below 100 °C in the microreformer, no reaction occurs, as evidenced in Fig. 14(e). As the fluid temperature continues to increase, there is no sudden change in temperature growth.

4.2.5. Optimal conditions for methanol steam reforming

In the previous sections, the methanol steam reforming process and its performance across various designs have been discussed. The investigations indicate that the helical spiral design exhibits superior performance, achieving faster conversion without the need for additional modifications compared to other approaches that require flow-altering designs to improve conversion rates. In this design, the reforming process operates optimally within the temperature range of 225–250 °C. Interestingly, this temperature range is achieved under varying conditions of supplied heat flux and S/C ratio for different designs. A critical finding suggests that designs with higher catalyst thickness experience significant pressure drops and thermal resistance due to the increased catalyst thickness, necessitating higher heat inputs

Table 4
Sample data points.

| S.N. | f_1 | f_2 |
|------|-------|-------|
| 1 | 0 | 3 |
| 2 | 1 | 2 |
| 3 | 2 | 1 |
| 4 | 3 | 0 |
| 5 | 1 | 3 |
| 6 | 2 | 2 |
| 7 | 3 | 1 |

Table 5
Pareto optimal points (marked Yes in last column) for minimization (f_1, f_2).

| S.N. | f_1 | f_2 | Pareto Front |
|------|-------|-------|--------------|
| 1 | 0 | 3 | Yes |
| 2 | 1 | 2 | Yes |
| 3 | 2 | 1 | Yes |
| 4 | 3 | 0 | Yes |
| 5 | 1 | 3 | No |
| 6 | 2 | 2 | No |
| 7 | 3 | 1 | No |

to maintain optimal reforming temperatures. Conversely, designs with lower catalyst thickness achieve the desired temperatures with lower heat flux and exhibit reduced pressure drops. Therefore, while designs with greater thickness favor higher r_{H_2} at increased heat flux, those with lower thickness enable faster conversion with less energy input. To identify the preferred design and operating conditions, a Pareto optimal front was Identified following the methodology outlined by Carlos & Coello [88].

The term 'Pareto' was introduced in the field of economics and named after the Italian economist V. Pareto in the 19th century [89]. In recent decades, however, it has broad application in computer science, spanning areas such as image processing, computer networks, machine learning, path planning, cloud computing, as well as the chemical and automotive industries. Pareto optimality serves as a mathematical framework for identifying non-dominated sets of feasible solutions, which are problem-specific. In the case of a minimization problem, the dominance relationship between two solutions, where y_1 dominates y_2 , is defined by Eq. (28) below:

$$f_i(y_1) \leq f_i(y_2) \quad \forall i \in \{1, 2, \dots, n\} \quad \text{and} \quad \exists j \in \{1, 2, \dots, n\} \mid f_j(y_1) < f_j(y_2) \quad (28)$$

In the case of a maximization problem, the dominance relationship between two solutions, where z_1 dominates z_2 , is represented by Eq. (29), as shown below:

$$f_i(z_1) \geq f_i(z_2) \quad \forall i \in \{1, 2, \dots, n\} \quad \text{and} \quad \exists j \in \{1, 2, \dots, n\} \mid f_j(z_1) > f_j(z_2) \quad (29)$$

Thus, for a minimization problem, a set of solutions can be said as non dominating (Pareto front) y^* , if no other solution dominates y^* (as identified by Eq. (28)). Conversely, in case of maximization problem, a set of solutions is considered non dominating/Pareto front z^* if no other solution dominates z^* (that can be identified by Eq. (29)). It is important to note that such sets of non-dominating solutions are referred to as the Pareto Front. Additionally, the Pareto Front can be either concave or convex depending on the solution space, as illustrated in Fig. 15. Fig. 15 (a and b) represent the minimization cases, while Fig. 15(c and d) correspond to the maximization cases.

Optimization can be viewed as a process for identifying a set of solutions that are incomparable. "Incomparable" refers to situations where it is difficult to determine which of two solutions is better when both need to be minimized. In other words, for two objectives, such as minimizing $f_1 = x$ and $f_2 = y$, selecting points where neither x nor y

can be further reduced without worsening the other is a key challenge. Optimization helps in identifying these sets of solutions that cannot be directly compared. To illustrate this, consider the following example:

Objective Functions: Let $f_1 = x$ and $f_2 = y$, where minimizing both functions means choosing points where neither x nor y can be reduced without adversely affecting the other.

Point Generation: The sample data points for x and y are listed in Table 4.

The non-dominated set for the minimization problem of (f_1, f_2), based on the data points discussed in Table 4, is detailed in Table 5. This table highlights the points that are part of the Pareto front, where each point is non-dominated, meaning no other point can improve one objective without worsening the other. Points identified as part of the Pareto front are marked with "Yes" in the last column.

Let's objectively consider each data points for possible selection and not being selected in Pareto front.

$x = 0, y = 3$ included in Pareto due to minimum in f_1 (lowest x).

$x = 1, y = 2$ included in Pareto due to incomparable in f_1 and f_2 non dominated.

$x = 2, y = 1$ included in Pareto due to incomparable in f_1 and f_2 non dominated.

$x = 3, y = 0$ included in Pareto due to minimum in f_1 (lowest x).

$x = 1, y = 3$ Dominated by $x = 1, y = 2$.

$x = 2, y = 2$ Dominated by $x = 3, y = 0$.

$x = 3, y = 1$ Dominated by $x = 2, y = 1$.

Extending Optimization for Three Objectives: For the three-objective optimization involving r_{H_2} , methanol conversion, and pressure drop, all objectives were converted into a maximization problem to ensure consistency. The pressure drop criterion was converted by negating its value, allowing it to be treated as a maximization objective.

Objective functions:

$f_1(z) = r_{H_2}$ # r_{H_2} to be maximize (z_1)

$f_2(z) = \text{Methanol conversion}$ # methanol conversion to be maximized (z_2)

$f_3(z) = -(\text{Pressure drop})$ # Pressure drop to be minimized (converted to maximization)

Algorithm: Identifying Pareto front for maximization

- Input >>> r_{H_2} , methanol conversion, pressure drop
- Output>>> Optimal set of feasible solution (Pareto Front)

Step 1: Create a uniform framework for the maximization problem:

$z_3^i = -y_3^j$ # Negate the pressure drop to convert it into a maximization problem

Step 2: Consider the updated objectives for the Pareto Front identification

Maximize [$w_1 f_1(z) + w_2 f_2(z) - w_3 f_3(z)$]

Equal weights were assigned to all outputs in the analysis.

Step 3: Identify the non dominating set of solutions k utilizing Eq. (29), such that:

$$f_1(k) \geq f_1(z), f_2(k) \geq f_2(z), \text{ and } z_3'(k) \geq z_3'(z)$$

Step 4: Pareto front: Output (f_1, f_2, f_3)

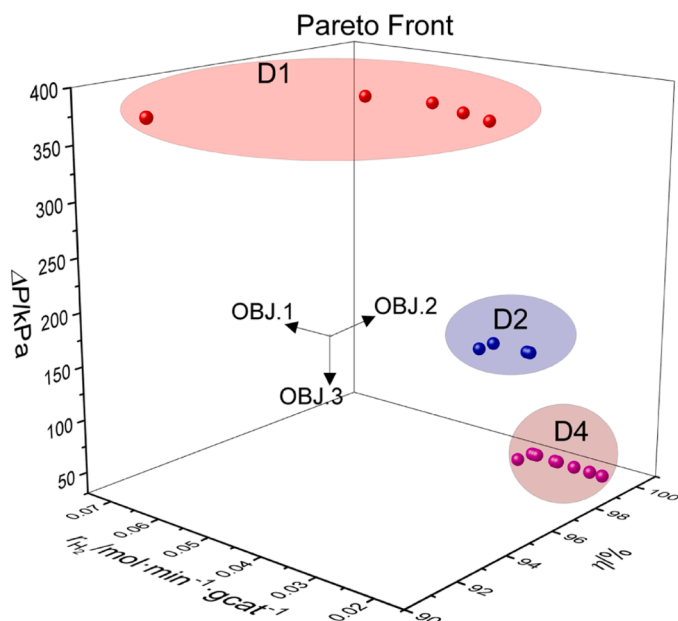


Fig. 16. Pareto Front analysis of optimal methanol steam reforming design.

The Pareto front includes f_1 and f_2 from the objective set, with the negated f_3 (f'_3) considered as the output.

MATLAB Implementation:

MATLAB 2024a was used to compute the Pareto front, considering the three objectives. This approach effectively identified the optimal solution set, providing insights into the trade-offs among r_{H_2} , methanol conversion, and pressure. The results offer a clear depiction of how multi-objective optimization aids in balancing competing engineering objectives, ensuring high performance and efficiency in the micro-reactor system.

The Pareto front analysis, illustrated in Fig. 16, identifies the optimal design conditions for the microreactor system. Designs D1, D2, and D4 emerge as high-performing configurations under specific operating parameters. Among these, Design D4 is considered the most cost-effective

solution due to its combination of lower catalyst usage, reduced pressure drop, and superior methanol conversion efficiency. Specifically, at an S/C ratio of 1, Design D4 results in a r_{H_2} of 0.034 and requiring a supplied heat flux of 300 W/m².

Observations on Dominated and Non-Dominated Solution Sets:

The non-dominated solutions (Fig. 16), identified using the algorithm discussed earlier, provide insights into achieving high performance while maintaining economic viability. A comparative analysis of these solutions was conducted through two approaches:

- Descriptive Statistics:** The descriptive statistics for each objective- r_{H_2} , methanol conversion, and pressure drop are shown in Fig. 17 (a-c). The analysis includes minimum, maximum, mean, and standard deviation (SD) values for both the dominated and non-dominated (Pareto front) solution sets. For r_{H_2} and methanol conversion (maximization objectives), the Pareto front solutions exhibit higher values compared to the dominated set (Fig. 17(a) and 17(b)). For pressure drop (minimization objective), no significant difference is evident (Fig. 17(c)). This could be due to the smaller number of solutions selected in the Pareto front, leading to reduced statistical variability in this objective.
- Visualization using Box-plots:** Box-plots for each objective, shown in Fig. 18(a-c), were used to compare the distributions of the dominated and non-dominated sets. For r_{H_2} and methanol conversion, the non-dominated solutions demonstrate consistently higher values across all statistics (Quartile 1, Quartile 2, Quartile 3, Min, and Max), indicating their superiority.

For pressure drop, the dominated set has lower values (Fig. 18(c)). This discrepancy could be attributed to: (i) Outliers in the dominated set, as marked in red in Fig. 18(c), which represent unusually high values excluded from the main data distribution. (ii) The smaller number of data points in the non-dominated set for pressure drop, potentially influenced by higher values from other objectives in the Pareto front.

Both descriptive statistics and box-plot analyses confirm that the Pareto front (non-dominated set) represents the optimal solution set for the microreactor system. These solutions maximize H_2 production and methanol conversion while minimizing pressure drop, offering superior performance and cost-efficiency compared to dominated solutions. The methodology provides a robust framework for optimizing multi-objective systems. This approach opens new possibilities for process

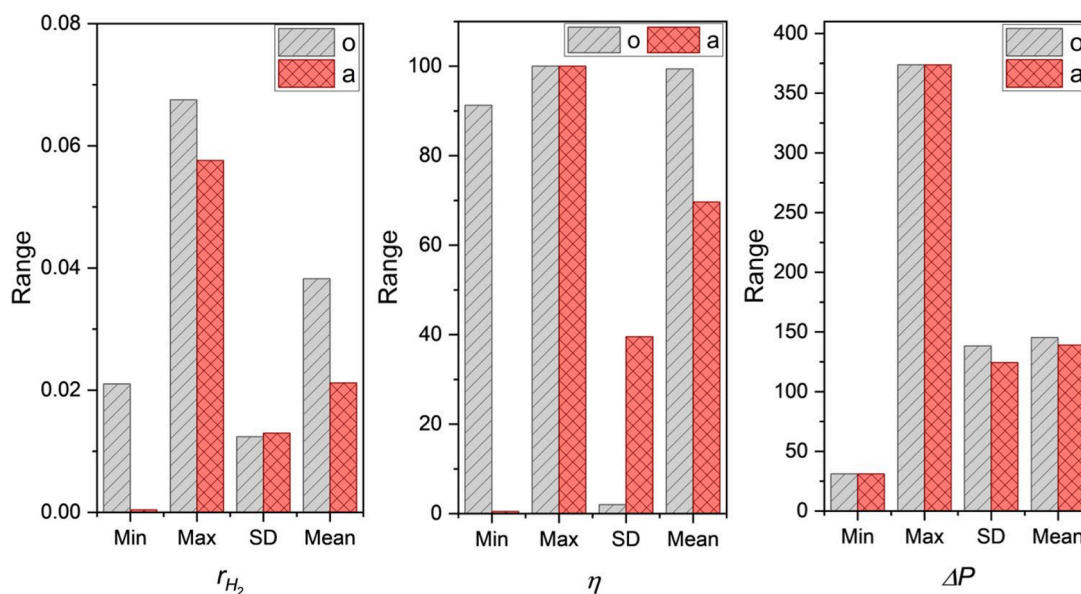


Fig. 17. Descriptive statistics comparing the non-dominating solution set (Pareto front or optimal, 'o') with the dominated set ('a') for the following outputs: (a) r_{H_2} , (b) Conversion performance, and (c) Pressure drop.

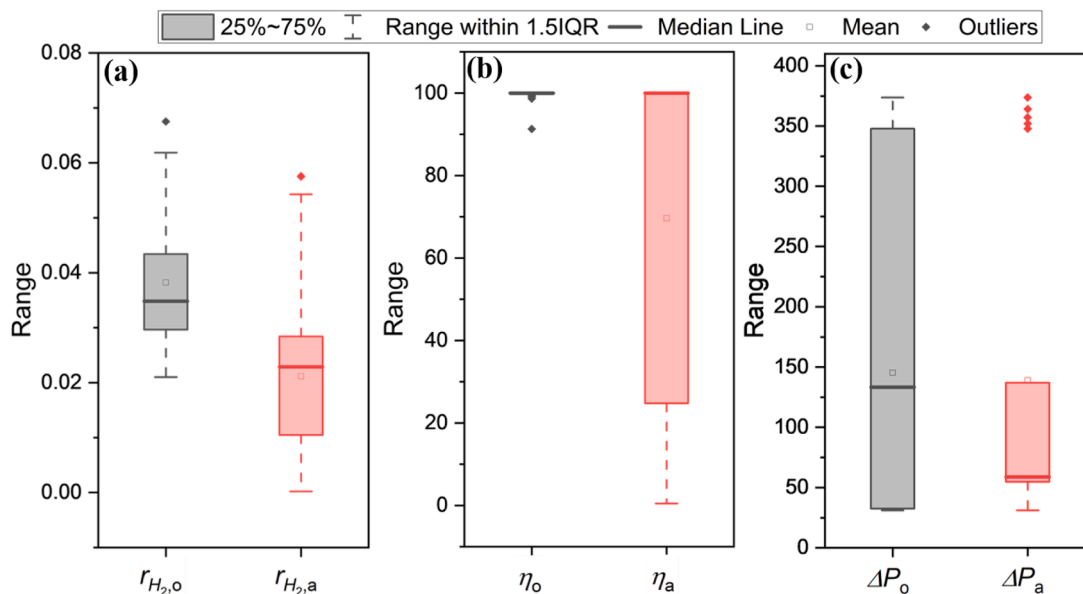


Fig. 18. Statistical analysis and distribution comparison of the non-dominating solution set (Pareto front or optimal, 'o') with the dominated set ('a') for the following outputs: (a) r_{H_2} , (b) Conversion performance, and (c) Pressure drop.

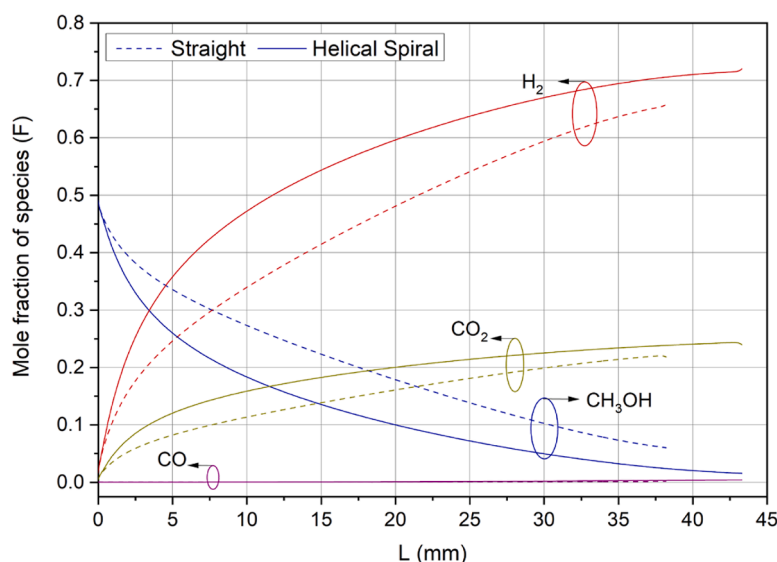


Fig. 19. Species product conversion along the arc length of the straight microreformer and the helical spiral microreformer.

intensification in H_2 production, offering insights into designing efficient and economically viable microreactors.

4.3. Comparison of the performance

It's important to analyze the physics formulation developed in the present study to evaluate its performance for other designs as well. The straight channel is a common case for steam reforming analysis in different scenarios. In the present simulation, we applied the developed model of the different coupled physics for solving the case of the microevaporator-microreformer system for the straight case as well. In the analysis, the total handling volume of the species mixture and hydraulic diameter remains the same as that of the helical design and is used to calculate the length of the straight cylindrical channel. Hence, the axial length of the straight cylindrical channel is equivalent to 38.2 mm for the evaporator and 38.2 mm for the microreformer, which is almost four times the axial length of the helical spiral.

The performance comparison between the helical and straight microreactor designs is conducted for the case where $S/C = 1$ and the heat flux is set to 500 W/m^2 , using a catalyst thickness of $62.5 \mu\text{m}$, corresponding to the D2 design of the helical spiral. Fig. 19 illustrates the species conversion performance comparison between the two microreactor designs. This investigation revealed that the helical spiral design facilitates faster methanol conversion compared to the straight design. Under these conditions of steam reforming, the methanol conversion in the straight cylindrical channel is approximately 87.75 %, whereas in the helical spiral design, it reaches 96.84 %, representing a significant improvement over the straight channel. Additionally, the mole fraction of the helical spiral design is notably higher at ~ 0.72 , compared to the straight cylindrical channel, which is ~ 0.65 .

Researchers have developed and investigated various designs to enhance the performance of steam reforming in microreactors. The present work utilizes a helical spiral microreactor design for both the evaporator and the microreformer. This proposed design is unique and

Table 6

Comparison of microreactor performance for methanol steam reforming across different studies.

| References | Microreformer structure | Catalyst | Catalyst thickness | S/C ratio | % max. conversion of fuel |
|----------------------|--|--|--------------------|-----------|---------------------------|
| Present study | Helical spiral | Cu/ZnO/ Al ₂ O ₃ | 37.5–75 μm | 1–3 | 100 % |
| Tadbir & Akbari [28] | Straight channel | Cu/ZnO/ Al ₂ O ₃ | 10–100 μm | 1–2 | 95 % |
| Ghodba et al. [68] | Array of straight microchannel | Cu/ZnO/ Al ₂ O ₃ | 100 μm | 1.1 | 93 % |
| Sarafriz et al. [91] | Parallel microchannel | Cu/SiO ₂ | – | 5 | 97 % |
| Liao et al. [92] | Cylindrical stricture | CuO/ ZnO/ CeO ₂ / ZrO ₂ / Al ₂ O ₃ | 2–20 μm | 1.2 | 94 % |
| Zhang et al. [93] | Straight channel | CuFeMg/ Al ₂ O ₃ | 100 μm | 2 | 99 % |
| Mei et al. [94] | micro-pin-fin arrays | Cu/ Zn ₂ O ₃ / Al ₂ O ₃ | 100 μm | 1–1.6 | 87.5 % |
| Delsman et al. [22] | Parallel channel | Cu/ZnO/ Al ₂ O ₃ | 100–200 | 1.2 | 99 % |
| Hafeez et al. [25] | Coated wall microreactor | Cu/ZnO/ Al ₂ O ₃ | 100 μm | 1.1 | 35–40 % |
| Fukahori et al. [75] | Tube shape microchannel | Cu/ZnO /Al ₂ O ₃ | – | 2 | 81.7 % |
| Xu et al. [95] | Porous copper fiber sintered felt (PCFS) | Cu | – | 1.3 | 96 % |
| Zhou et al. [96] | Small-S, Medium-M, and Large-L | Cu/Zn/ Al/Zr | – | 1.3 | ≈95 % |
| Wu et al. [97] | Stacked wave sheet type | Pt/Al ₂ O ₃ | – | 1.5 | 65 % |
| Wang et al. [51] | Honeycomb | SiC | 360 μm | 1.2 | 98.7 % |
| Baydir and Aras [47] | Parallel microchannel | Cu/ZnO | – | 1–1.8 | 94 % |
| Zhou et al. [98] | Flexible tubular microreactor | CuO\ZnO \Al ₂ O ₃ | – | 1.3 | 84.91 % |

represents the first coupled study of the microevaporator and the reformer. Table 6 indicates the comparison between the microreactor performance of different studies, detailing the design utilized, the type of catalyst used, its thickness, and S/C ratio, along with the obtained maximum conversion. In all of the studies, an S/C ratio above 1 was chosen to enhance the conversion of methanol. The majority of the studies reported methanol conversions above 90 %. Furthermore, the Cu/ZnO/Al₂O₃ catalyst, widely recognized for methanol steam reforming, was commonly selected, consistent with our present work. Additionally, most studies opted for a wall-coated catalyst configuration for the microreformer. As depicted in Table 6, despite variations in assumptions across other studies, the present work closely simulates the actual reforming scenario in the helical spiral-shaped microreactor. This design enables rapid methanol conversion within a short length, outperforming other designs. The selection of this design is attributed to its high catalytic activity in the wall-coated configuration [25], which also entails lesser pressure drop compared to packed bed reactors [90].

5. Conclusion

In this work, a comprehensive evaluation of the performance of a helical spiral microevaporator-microreformer coupled system was conducted. The proposed coupled system demonstrates high efficiency in producing H₂ and achieving a high conversion of methanol into the desired product. The main conclusions of this work are as follows:

Performance of microreactor:

- In the proposed design of the helical spiral microreactor, complete conversion of methanol is achieved rapidly. The present design outperforms other configurations, enabling fast conversion of methanol (achieving 100 % conversion) in a short length.
- The design with a smaller catalyst thickness facilitates the fastest conversion, with complete methanol conversion occurring in just one-fifth of the length of the microreformer. Conversely, a thicker catalyst layer necessitates a longer length for full conversion.

Impact of Different Parameters:

- Numerical simulations investigated the effects of catalyst layer thickness, supplied heat flux, and S/C ratio. The design with varying catalyst thickness allows complete conversion under different combinations of heat flux and supplied S/C ratio. The low catalyst thickness design allows full conversion at relatively lower heat flux compared to the high catalyst thickness design, but the high catalyst thickness design yields higher r_{H_2} values.
- In the low thickness catalyst design, most methanol is consumed earlier, with a slight increase in CO mole fraction as the supplied heat flux increases.
- A higher S/C ratio accelerates methanol conversion, but only marginally affects H₂ production, while decreasing CO production. A slight decrease in H₂ mole fraction is observed as the S/C ratio increases.

Temperature and Pressure considerations:

- The endothermic nature of methanol steam reforming causes a temperature drop when the methanol-water mixture enters the microreformer. This temperature drop results from the net energy required for the reaction and the amount of supplied energy.
- Increasing heat flux speeds up conversion, leading to higher mixture temperatures. The temperature range of 225–250 °C favors methanol steam reforming, and the reaction tends to reach this temperature to achieve equilibrium conditions.
- In the low thickness design with high heat flux case, the reaction is observed to start before entering the microreformer.
- The high thickness design also demonstrates a relatively larger pressure drop compared to the low thickness design.

Optimal Design and Future direction:

- Analysis shows that among all designs, D4 is optimal due to its cost-effective catalyst use, low heat input, and high methanol conversion efficiency with the favored optimal operating conditions of S/C ratio of 1 and 300 W/m² heat flux.

The proposed design provides insights into the coupled operation of a single-channel microevaporator-microreformer system, enabling a compact and simplified structure with potential industrial applications. Future work will focus on scaling the current design to enhance H₂ production and evaluating its efficiency and scalability compared to traditional methods.

CRediT authorship contribution statement

Devendra Yadav: Writing – original draft, Validation, Software, Methodology, Investigation, Data curation, Conceptualization. **Xinlong Lu:** Visualization, Validation, Software, Formal analysis, Data curation. **Prabhat Dansena:** Writing – original draft, Methodology, Data curation. **Dengwei Jing:** Writing – review & editing, Supervision, Methodology, Funding acquisition, Conceptualization.

Declaration of competing interest

The authors declare that they have no known competing financial interests or personal relationships that could have appeared to influence the work reported in this paper.

Acknowledgments

The authors gratefully acknowledge financial support from the National Natural Science Foundation of China (No. 52025061), the Zhuhai Innovation and Entrepreneurship Team Project (No. 2120004000225), the Shaanxi Provincial Science and Technology Innovation Team (No. 2023-CX-TD25), and the China Fundamental Research Funds for the Central Universities.

Data availability

Data will be made available on request.

References

- J.C. Amphlett, K.A.M. Creber, J.M. Davis, R.F. Mann, B.A. Peppley, D.M. Stokes, Hydrogen production by steam reforming of methanol for polymer electrolyte fuel cells, *Int. J. Hydrogen Energy*. 19 (1994) 131–137, [https://doi.org/10.1016/0360-3199\(94\)90117-1](https://doi.org/10.1016/0360-3199(94)90117-1).
- A.Q. Al Shetwi, Sustainable development of renewable energy integrated power sector: trends, environmental impacts, and recent challenges, *Sci. Total Environ.* 822 (2022) 153645, <https://doi.org/10.1016/j.scitotenv.2022.153645>.
- H. Hamada, Y. Kusayanagi, M. Tatsumatsu, M. Watanabe, H. Kikusato, Challenges for a reduced inertia power system due to the large-scale integration of renewable energy, *Glob. Energy Interconnect.* 5 (2022) 266–273, <https://doi.org/10.1016/j.gloei.2022.06.003>.
- S. Singh, S. Jain, P.S. V., A.K. Tiwari, M.R. Nouni, J.K. Pandey, S. Goel, Hydrogen: a sustainable fuel for future of the transport sector, *Renew. Sustain. Energy Rev.* 51 (2015) 623–633, <https://doi.org/10.1016/j.rser.2015.06.040>.
- A. Roy, S. Pramanik, A review of the hydrogen fuel path to emission reduction in the surface transport industry, *Int. J. Hydrogen Energy*. (2023), <https://doi.org/10.1016/j.ijhydene.2023.07.010>.
- A. González, E. McKeogh, B.O. Gallachóir, The role of hydrogen in high wind energy penetration electricity systems: the Irish case, *Renew. Energy*. 29 (2004) 471–489, <https://doi.org/10.1016/j.renene.2003.07.006>.
- T.R. Hawkins, B. Singh, G. Majeau-Bettez, A.H. Strømman, Comparative environmental life cycle assessment of conventional and electric vehicles, *J. Ind. Ecol.* 17 (2013) 53–64, <https://doi.org/10.1111/j.1530-9290.2012.00532.x>.
- M. Coffman, P. Bernstein, S. Wee, Electric vehicles revisited: a review of factors that affect adoption, *Transp. Rev.* 37 (2017) 79–93, <https://doi.org/10.1080/01441647.2016.1217282>.
- C.-Y. Hsueh, H.-S. Chu, W.-M. Yan, C.-H. Chen, Numerical study of heat and mass transfer in a plate methanol steam micro reformer with methanol catalytic combustor, *Int. J. Hydrogen Energy*. 35 (2010) 6227–6238, <https://doi.org/10.1016/j.ijhydene.2010.03.036>.
- A. Fazeli, M. Behnam, Hydrogen production in a zigzag and straight catalytic wall coated micro channel reactor by CFD modeling, *Int. J. Hydrogen Energy*. 35 (2010) 9496–9503, <https://doi.org/10.1016/j.ijhydene.2010.05.052>.
- M. de-Souza, G.M. Zanin, F.F. Moraes, Parametric study of hydrogen production from ethanol steam reforming in a membrane microreactor, *Brazilian J. Chem. Eng.* 30 (2013) 355–367, <https://doi.org/10.1590/S0104-66322013000200013>.
- Y. Li, S. Kimura, Economic competitiveness and environmental implications of hydrogen energy and fuel cell electric vehicles in ASEAN countries: the current and future scenarios, *Energy Policy* 148 (2021) 111980, <https://doi.org/10.1016/j.enpol.2020.111980>.
- K. Hbaieb, K.K.A. Rashid, F. Kooli, Hydrogen production by autothermal reforming of dodecane over strontium titanate based perovskite catalysts, *Int. J. Hydrogen Energy*. 42 (2017) 5114–5124, <https://doi.org/10.1016/j.ijhydene.2016.11.127>.
- E.C. Vagia, N. Muradov, A. Kalyva, A. T-Raissi, N. Qin, A.R. Srinivasa, K. E. Kakosimos, Solar hybrid photo-thermochemical sulfur-ammonia water-splitting cycle: photocatalytic hydrogen production stage, *Int. J. Hydrogen Energy*. 42 (2017) 20608–20624, <https://doi.org/10.1016/j.ijhydene.2017.06.210>.
- S.E. Hosseini, M.A. Wahid, Hydrogen production from renewable and sustainable energy resources: promising green energy carrier for clean development, *Renew. Sustain. Energy Rev.* 57 (2016) 850–866, <https://doi.org/10.1016/j.rser.2015.12.112>.
- P. Sivagurunathan, G. Kumar, T. Kobayashi, K. Xu, S.-H. Kim, Effects of various dilute acid pretreatments on the biochemical hydrogen production potential of marine macroalgal biomass, *Int. J. Hydrogen Energy*. 42 (2017) 27600–27606, <https://doi.org/10.1016/j.ijhydene.2017.05.106>.
- P.J. Megía, A.J. Vizcaino, J.A. Calles, A. Carrero, Hydrogen Production Technologies: from Fossil Fuels toward Renewable Sources. A Mini Review, *Energy & Fuels* 35 (2021) 16403–16415, <https://doi.org/10.1021/acs.energyfuels.1c02501>.
- P. Nikolaidis, A. Poullikkas, A comparative overview of hydrogen production processes, *Renew. Sustain. Energy Rev.* 67 (2017) 597–611, <https://doi.org/10.1016/j.rser.2016.09.044>.
- D. Yadav, X. Lu, C.B. Vishwakarma, D. Jing, Advancements in microreactor technology for hydrogen production via steam reforming: a comprehensive review of experimental studies, *J. Power Sources*. 585 (2023) 233621, <https://doi.org/10.1016/j.jpowsour.2023.233621>.
- F. Muellerlanger, E. Tzimas, M. Kaltschmitt, S. Petevs, Techno-economic assessment of hydrogen production processes for the hydrogen economy for the short and medium term, *Int. J. Hydrogen Energy*. 32 (2007) 3797–3810, <https://doi.org/10.1016/j.ijhydene.2007.05.027>.
- D. Yadav, X. Lu, B.-C. Ma, D. Jing, Advancements in microreactor technology for hydrogen production via steam reforming: a comprehensive review of numerical studies, *J. Power Sources*. 596 (2024) 234090, <https://doi.org/10.1016/j.jpowsour.2024.234090>.
- E.R. Delsman, B.J.P.F. Laarhoven, M.H.J.M. De Croon, G.J. Kramer, J.C. Schouten, Comparison between conventional fixed-bed and microreactor technology for a portable hydrogen production case, *Chem. Eng. Res. Des.* 83 (2005) 1063–1075, <https://doi.org/10.1205/cherd.04260>.
- J. Wei, E. Iglesia, Mechanism and Site Requirements for Activation and Chemical Conversion of Methane on Supported Pt Clusters and Turnover Rate Comparisons among Noble Metals, *J. Phys. Chem. B* 108 (2004) 4094–4103, <https://doi.org/10.1021/jp036985z>.
- S. Kim, S.-W. Yun, B. Lee, J. Heo, K. Kim, Y.-T. Kim, H. Lim, Steam reforming of methanol for ultra-pure H₂ production in a membrane reactor: techno-economic analysis, *Int. J. Hydrogen Energy*. 44 (2019) 2330–2339, <https://doi.org/10.1016/j.ijhydene.2018.08.087>.
- S. Hafeez, E. Aristodemou, G. Manos, S.M. Al-Salem, A. Constantinou, Modelling of packed bed and coated wall microreactors for methanol steam reforming for hydrogen production, *RSC Adv* 10 (2020) 41680–41692, <https://doi.org/10.1039/d0ra06834a>.
- S.R. Deshmukh, A.B. Mhadeshwar, D.G. Vlachos, Microreactor Modeling for Hydrogen Production from Ammonia Decomposition on Ruthenium, *Ind. Eng. Chem. Res.* 43 (2004) 2986–2999, <https://doi.org/10.1021/ie030557y>.
- M. Andisheh Tadbir, M.H. Akbari, Integrated methanol reforming and oxidation in wash-coated microreactors: a three-dimensional simulation, *Int. J. Hydrogen Energy*. 37 (2012) 2287–2297, <https://doi.org/10.1016/j.ijhydene.2011.11.015>.
- M.A. Tadbir, M.H. Akbari, Methanol steam reforming in a planar wash coated microreactor integrated with a micro-combustor, *Int. J. Hydrogen Energy*. 36 (2011) 12822–12832, <https://doi.org/10.1016/j.ijhydene.2011.05.010>.
- J. Agrell, H. Birgersson, M. Boutonnet, Steam reforming of methanol over a Cu/ZnO/Al₂O₃ catalyst: a kinetic analysis and strategies for suppression of CO formation, *J. Power Sources*. 106 (2002) 249–257, [https://doi.org/10.1016/S0378-7753\(01\)01027-8](https://doi.org/10.1016/S0378-7753(01)01027-8).
- M. Lee, R. Greif, C.P. Grigoropoulos, H.G. Park, F.K. Hsu, Transport in packed-bed and wall-coated steam-methanol reformers, *J. Power Sources*. 166 (2007) 194–201, <https://doi.org/10.1016/j.jpowsour.2007.01.007>.
- X. Chu, X. Zeng, T. Zheng, W. Zhuang, Y. Yang, W. Zhou, Y. Hong, Structural design and performance research of methanol steam reforming microchannel for hydrogen production based on mixing effect, *Int. J. Hydrogen Energy*. 45 (2020) 20859–20874, <https://doi.org/10.1016/j.ijhydene.2020.05.190>.
- T. Zheng, W. Zhou, Y. Yang, Y. Zhong, H. You, X. Li, X. Chu, K.S. Hui, W. Ding, Novel Nickel Foam with Multiple Microchannels as Combustion Reaction Support for the Self-Heating Methanol Steam Reforming Microreactor, *Energy and Fuels* 35 (2021) 2815–2825, <https://doi.org/10.1021/acs.energyfuels.0c02712>.
- K. Yoshida, S. Tanaka, H. Hiraki, M. Esashi, A micro fuel reformer integrated with a combustor and a microchannel evaporator, *J. Micromechanics Microengineering*. 16 (2006), <https://doi.org/10.1088/0960-1317/16/9/S04>.
- Y. Wang, Q. Wu, D. Mei, Y. Wang, Development of highly efficient methanol steam reforming system for hydrogen production and supply for a low temperature proton exchange membrane fuel cell, *Int. J. Hydrogen Energy*. 45 (2020) 25317–25327, <https://doi.org/10.1016/j.ijhydene.2020.06.285>.
- Y. Chen, C. Zhang, R. Wu, M. Shi, Methanol steam reforming in microreactor with constructal tree-shaped network, *J. Power Sources*. 196 (2011) 6366–6373, <https://doi.org/10.1016/j.jpowsour.2011.03.044>.
- X. Zhuang, X. Xu, L. Li, D. Deng, Numerical investigation of a multichannel reactor for syngas production by methanol steam reforming at various operating conditions, *Int. J. Hydrogen Energy*. 45 (2020) 14790–14805, <https://doi.org/10.1016/j.ijhydene.2020.03.207>.
- S. Hu, X. Cui, L. Yang, Thermal matching characteristics in an autothermal methanol reforming microchannel reactor for hydrogen production, *Chem. Eng. Sci.* 280 (2023) 118987, <https://doi.org/10.1016/j.ces.2023.118987>.
- J. Chen, Y. Yu, Numerical modelling for design of microchannel reactors: application to hydrogen production from methanol by steam reforming, *Int. J.*

- Hydrogen Energy. 50 (2024) 1526–1540, <https://doi.org/10.1016/j.ijhydene.2023.11.061>.
- [39] J. Chen, Hydrogen production in protruded millisecond microchannel reactors by catalytically reforming methanol, *Int. J. Hydrogen Energy*. 67 (2024) 225–239, <https://doi.org/10.1016/j.ijhydene.2024.04.152>.
- [40] H. Yang, G. Yao, D. Wen, Flow resistance and convective heat transfer by elastic turbulence in 1D/2D/3D geometries, *Int. J. Therm. Sci.* 176 (2022) 107512, <https://doi.org/10.1016/j.ijthermalsci.2022.107512>.
- [41] J. Wang, Y. Zhang, S. Peng, S. Yu, J. Ran, K.J. Chua, M. Li, Yunlin Shao, S. Liu, Thermal analysis of a micro tubular reactor for methanol steam reforming by optimizing the multilayer arrangement of catalyst bed for the catalytic combustion of methanol, *Int. J. Hydrogen Energy*. 48 (2023) 28315–28332, <https://doi.org/10.1016/j.ijhydene.2023.03.450>.
- [42] T. Kim, S. Kwon, Design, fabrication and testing of a catalytic microreactor for hydrogen production, *J. Micromechanics Microengineering*. 16 (2006) 1752–1760, <https://doi.org/10.1088/0960-1317/16/9/002>.
- [43] J. Chen, T. Li, Design Issues of Thermally Integrated Methanol Reforming Systems for the Production of Hydrogen: effects of Channel Dimensions and Catalyst Properties, *Energy & Fuels* 33 (2019) 12026–12040, <https://doi.org/10.1021/acs.energyfuels.9b02836>.
- [44] F. Qureshi, F. Ahmad, M. Idrees, A.A. Khan, S. Zaidi, Simulation of methanol steam reforming process for the production of hydrogen, *Indian Chem. Eng.* 63 (2021) 99–116, <https://doi.org/10.1080/00194506.2019.1689186>.
- [45] C.-Y. Hsueh, H.-S. Chu, W.-M. Yan, C.-H. Chen, Transport phenomena and performance of a plate methanol steam micro-reformer with serpentine flow field design, *Appl. Energy*. 87 (2010) 3137–3147, <https://doi.org/10.1016/j.apenergy.2010.02.027>.
- [46] J. Chen, L. Yan, W. Song, D. Xu, Methane steam reforming thermally coupled with catalytic combustion in catalytic microreactors for hydrogen production, *Int. J. Hydrogen Energy*. 42 (2017) 664–680, <https://doi.org/10.1016/j.ijhydene.2016.12.114>.
- [47] E. Baydir, Ö. Aras, Methanol steam reforming in a microchannel reactor coated with spray pyrolysis method for durable Cu/ZnO nanocatalyst, *J. Anal. Appl. Pyrolysis*. 158 (2021) 105278, <https://doi.org/10.1016/j.jaap.2021.105278>.
- [48] H. Purnama, T. Ressler, R. Jentoft, H. Soerijanto, R. Schlögl, R. Schomäcker, CO formation/selectivity for steam reforming of methanol with a commercial CuO/ZnO/Al₂O₃ catalyst, *Appl. Catal. A Gen.* 259 (2004) 83–94, <https://doi.org/10.1016/j.apcata.2003.09.013>.
- [49] R.C. Pattison, F.E. Estep, M. Baldea, Pseudodistributed feed configurations for catalytic plate microchannel reactors, *Ind. Eng. Chem. Res.* 53 (2014) 5028–5037, <https://doi.org/10.1021/ie4008997>.
- [50] Y.W. Budhi, H. Devianto, F. Mahardhika, L. Ignacia, H.A. Mikhael, Fluid dynamics and kinetic simulation for steam reforming of ethanol using a microchannel reactor, in: 2014 Int. Conf. Electr. Eng. Comput. Sci., IEEE, 2014, pp. 85–90, <https://doi.org/10.1109/ICEECS.2014.7045225>.
- [51] Y. Wang, H. Liu, D. Mei, Q. Wu, H. Zhou, A novel thermally autonomous methanol steam reforming microreactor using SiC honeycomb ceramic as catalyst support for hydrogen production, *Int. J. Hydrogen Energy*. 46 (2021) 25878–25892, <https://doi.org/10.1016/j.ijhydene.2021.05.103>.
- [52] D.G. Norton, E.D. Wetzel, D.G. Vlachos, Thermal management in catalytic microreactors, *Ind. Eng. Chem. Res.* 45 (2006) 76–84, <https://doi.org/10.1021/ie050674o>.
- [53] G.D. Stefanidis, D.G. Vlachos, Millisecond methane steam reforming via process and catalyst intensification, *Chem. Eng. Technol.* 31 (2008) 1201–1209, <https://doi.org/10.1002/ceat.200800237>.
- [54] M. Qian, D. Mei, Z. Yi, Y. Feng, Z. Chen, Fluid flow and heat transfer performance in a micro-reactor with non-uniform micro-pin-fin arrays for hydrogen production at low Reynolds number, *Int. J. Hydrogen Energy*. 42 (2017) 553–561, <https://doi.org/10.1016/j.ijhydene.2016.10.150>.
- [55] R. G. D. Muniyappan, A. Ramanathan, Biodiesel production using microreactor with integrated microheater through multi-objective optimization approach, *Chem. Eng. Process. - Process Intensif.* 195 (2024) 109646, <https://doi.org/10.1016/j.cep.2023.109646>.
- [56] H. Osman, S.H. Hosseini, K. Elsayed, CFD modelling and multi-objective optimization of MHO for hydrodynamic cavitation generator using a radial basis function neural network, and NSGA-II, *Chem. Eng. Process. - Process Intensif.* 190 (2023) 109416, <https://doi.org/10.1016/j.cep.2023.109416>.
- [57] A. Agrawal, B.R. Bakshi, H. Kodamana, M. Ramteke, Multi-objective optimization of food-energy-water nexus via crops land allocation, *Comput. Chem. Eng.* 183 (2024) 108610, <https://doi.org/10.1016/j.compchemeng.2024.108610>.
- [58] A. Haq, R. Sharma, B.R. Bakshi, H. Kodamana, M. Ramteke, Forecasting sustainable power generation profiles to achieve net zero emissions using multi-objective techno-ecological framework: a study in the context of India, *Comput. Chem. Eng.* 179 (2023) 108439, <https://doi.org/10.1016/j.compchemeng.2023.108439>.
- [59] H. Chen, P. Yu, J. Long, Multi-objective optimization of automotive seat frames using machine learning, *Adv. Eng. Softw.* 199 (2025) 103797, <https://doi.org/10.1016/j.advengsoft.2024.103797>.
- [60] Y. Wang, T. Zhang, L. Chen, W. Tao, Multi-objective optimization of laser perforated fuel filter parameters based on artificial neural network and genetic algorithm, *Particuology* 96 (2025) 57–70, <https://doi.org/10.1016/j.partic.2024.10.016>.
- [61] F. Li, L. Liu, Y. Yu, Deep reinforcement learning-based multi-objective optimization for electricity-gas-heat integrated energy systems, *Expert Syst. Appl.* 262 (2025) 125558, <https://doi.org/10.1016/j.eswa.2024.125558>.
- [62] J. Nie, Z. Liu, J. Su, C. Zhang, Y. Li, Multi-objective optimization of liquid cooling system for lithium-ion battery, *J. Energy Storage*. 103 (2024) 114380, <https://doi.org/10.1016/j.est.2024.114380>.
- [63] K. Chai, W. Xia, R. Shen, G. Luo, Y. Cheng, W. Su, A. Su, Optimization of heterogeneous continuous flow hydrogenation using FTIR inline analysis: a comparative study of multi-objective Bayesian optimization and kinetic modeling, *Chem. Eng. Sci.* 302 (2025) 120901, <https://doi.org/10.1016/j.ces.2024.120901>.
- [64] Y. Tang, W. Long, Y. Wang, G. Xiao, Y. Wang, M. Lu, Multi-objective optimization of methanol reforming reactor performance based on response surface methodology and multi-objective particle swarm optimization coupling algorithm for on-line hydrogen production, *Energy Convers. Manag.* 307 (2024) 118377, <https://doi.org/10.1016/j.enconman.2024.118377>.
- [65] Y. Wang, Z. Hong, D. Mei, A thermally autonomous methanol steam reforming microreactor with porous copper foam as catalyst support for hydrogen production, *Int. J. Hydrogen Energy*. 46 (2021) 6734–6744, <https://doi.org/10.1016/j.ijhydene.2020.11.111>.
- [66] D. Pashchenko, A. Eremin, Heat flow inside a catalyst particle for steam methane reforming: cFD-modeling and analytical solution, *Int. J. Heat Mass Transf.* 165 (2021) 120617, <https://doi.org/10.1016/j.ijheatmasstransfer.2020.120617>.
- [67] A. Abidi, A. Ahmadi, M. Enayati, S. Sajadi, H. Yarmand, A. Ahmed, G. Cheraghian, A review of the methods of modeling multi-phase flows within different microchannels shapes and their applications, *Micromachines (Basel)* 12 (2021) 1113, <https://doi.org/10.3390/mi12091113>.
- [68] A. Ghodba, M. Sharifzadeh, D. Rashtchian, Integrated and inherently safe design and operation of a mobile power generation: process intensification through microreactor reformer and HT-PEMFC, *Int. J. Hydrogen Energy*. 46 (2021) 23839–23854, <https://doi.org/10.1016/j.ijhydene.2021.04.176>.
- [69] B.J. Bayly, C.D. Levermore, T. Passot, Density variations in weakly compressible flows, *Phys. Fluids A*. 4 (1992) 945–954, <https://doi.org/10.1063/1.858275>.
- [70] R. Capuano, T. Fend, B. Hoffschmidt, R. Pitz-Paal, Innovative volumetric solar receiver micro-design based on numerical predictions, in: ASME Int. Mech. Eng. Congr. Expo. Proc., 2015, pp. 1–10, <https://doi.org/10.1115/IMECE2015-50597>.
- [71] N. Solehati, J. Bae, A.P. Sasmito, Numerical investigation of mixing performance in microchannel T-junction with wavy structure, *Comput. Fluids*. 96 (2014) 10–19, <https://doi.org/10.1016/j.compfluid.2014.03.003>.
- [72] H. Van Phan, M.B. Coşkun, M. Şeşen, G. Pandraud, A. Neild, T. Alan, Vibrating membrane with discontinuities for rapid and efficient microfluidic mixing, *Lab Chip* 15 (2015) 4206–4216, <https://doi.org/10.1039/C5LC00836K>.
- [73] L.E.N. Bird, B. R. W.E. Stewart, *Transport Phenomena*, John Wiley & Sons, Inc., New York, 2002. Second Ed.
- [74] Y.R. Lu, D. Pashchenko, P.A. Nikrityuk, A new semiempirical model for the heat and mass transfer inside a spherical catalyst in a stream of hot CH₄/H₂O gases, *Chem. Eng. Sci.* 238 (2021) 116565, <https://doi.org/10.1016/j.ces.2021.116565>.
- [75] S. Fukahori, H. Koga, T. Kitaoka, M. Nakamura, H. Wariishi, Steam reforming behavior of methanol using paper-structured catalysts: experimental and computational fluid dynamic analysis, *Int. J. Hydrogen Energy*. 33 (2008) 1661–1670, <https://doi.org/10.1016/j.ijhydene.2007.12.063>.
- [76] F. Chen, M.H. Chang, C.Y. Kuo, C.Y. Hsueh, W.M. Yan, Analysis of a plate-type microreformer for methanol steam reforming reaction, *Energy and Fuels* 23 (2009) 5092–5098, <https://doi.org/10.1021/ef9005252>.
- [77] J.D. Holladay, Y. Wang, E. Jones, Review of developments in portable hydrogen production using microreactor technology, *Chem. Rev.* 104 (2004) 4767–4789, <https://doi.org/10.1021/cr020721b>.
- [78] K. Ghasemzadeh, S. Liguori, P. Morrone, A. Iulianelli, V. Piemonte, A.A. Babaluo, A. Basile, H₂ production by low pressure methanol steam reforming in a dense Pd–Ag membrane reactor in co-current flow configuration: experimental and modeling analysis, *Int. J. Hydrogen Energy*. 38 (2013) 16685–16697, <https://doi.org/10.1016/j.ijhydene.2013.06.001>.
- [79] A.V.A.V. Pattekar, M.V.M.V.M.V. Kothare, A Microreactor for Hydrogen Production in Micro Fuel Cell Applications, *J. Microelectromechanical Syst.* 13 (2004) 7–18, <https://doi.org/10.1109/JMEMS.2004.823224>.
- [80] L. Carlson, C. Eric, Aspen technology, don't gamble with physical properties for simulations, *Chem. Eng. Prog.* (1996) 35–46.
- [81] J.-S. Suh, M. Lee, R. Greif, C.P. Grigoropoulos, A study of steam methanol reforming in a microreactor, *J. Power Sources*. 173 (2007) 458–466, <https://doi.org/10.1016/j.jpowsour.2007.04.038>.
- [82] M.S. Herdem, M. Mundhwa, S. Farhad, F. Hamdullahpur, Catalyst layer design and arrangement to improve the performance of a microchannel methanol steam reformer, *Energy Convers. Manag.* 180 (2019) 149–161, <https://doi.org/10.1016/j.enconman.2018.10.094>.
- [83] H.G. Park, J.A. Malen, W.T. Piggott, J.D. Morse, R. Greif, C.P. Grigoropoulos, M. A. Havstad, R. Upadhye, Methanol steam reformer on a silicon wafer, *J. Microelectromechanical Syst.* 15 (2006) 976–985, <https://doi.org/10.1109/JMEMS.2006.878888>.
- [84] D. Lesmana, H.S. Wu, Cu/ZnO/Al₂O₃/Cr₂O₃/CeO₂ catalyst for hydrogen production by oxidative methanol reforming via washcoat catalyst preparation in microchannel reactor, *Bull. Chem. React. Eng. Catal.* 12 (2017) 384–392, <https://doi.org/10.9767/bcrec.12.3.966.384-392>.
- [85] D. Pashchenko, I. Makarov, Carbon deposition in steam methane reforming over a Ni-based catalyst: experimental and thermodynamic analysis, *Energy* 222 (2021) 119993, <https://doi.org/10.1016/j.energy.2021.119993>.
- [86] D. Pashchenko, Intra-particle diffusion limitation for steam methane reforming over a Ni-based catalyst, *Fuel* 353 (2023) 129205, <https://doi.org/10.1016/j.fuel.2023.129205>.

- [87] F. Chen, M.-H. Chang, C.-W. Hsu, Analysis of membraneless microfuel cell using decomposition of hydrogen peroxide in a Y-shaped microchannel, *Electrochim. Acta*. 52 (2007) 7270–7277, <https://doi.org/10.1016/j.electacta.2007.05.072>.
- [88] C.A. Coello, Coello Coello, A short tutorial on evolutionary multiobjective optimization, in: *Lect. Notes Comput. Sci.*, Springer, Berlin Heidelberg, 2001, pp. 21–40, https://doi.org/10.1007/3-540-44719-9_2.
- [89] S. Brisset, F. Gillon, Approaches for multi-objective optimization in the ecodesign of electric systems, *Eco-Friendly Innov. Electr. Transm. Distrib. Networks*. (2015) 83–97, <https://doi.org/10.1016/B978-1-78242-010-1.00004-5>.
- [90] A. Karim, J. Bravo, D. Gorm, T. Conant, A. Datye, Comparison of wall-coated and packed-bed reactors for steam reforming of methanol, *Catal. Today*. 110 (2005) 86–91, <https://doi.org/10.1016/j.cattod.2005.09.010>.
- [91] M.M. Sarafraz, M.R. Safaei, M. Goodarzi, M. Arjomandi, Experimental investigation and performance optimisation of a catalytic reforming micro-reactor using response surface methodology, *Energy Convers. Manag.* 199 (2019) 111983, <https://doi.org/10.1016/j.enconman.2019.111983>.
- [92] M. Liao, H. Qin, W. Guo, P. Gao, H. Xiao, In Situ Reduction of a CuO/ZnO/CeO₂/ZrO₂ Catalyst Washcoat Supported on Al₂O₃ Foam Ceramic by Glycerol for Methanol Steam Reforming in a Microreactor, *Ind. Eng. Chem. Res* 60 (2021) 8991–9001, <https://doi.org/10.1021/acs.iecr.1c01180>.
- [93] G. Zhang, J. Zhao, Q. Wang, T. Yang, Q. Zhang, L. Zhang, Fast start-up structured CuFeMg/Al₂O₃ catalyst applied in microreactor for efficient hydrogen production in methanol steam reforming, *Chem. Eng. J.* 426 (2021) 130644, <https://doi.org/10.1016/j.cej.2021.130644>.
- [94] D. Mei, M. Qian, B. Liu, B. Jin, Z. Yao, Z. Chen, A micro-reactor with micro-pin-fin arrays for hydrogen production via methanol steam reforming, *J. Power Sources*. 205 (2012) 367–376, <https://doi.org/10.1016/j.jpowsour.2011.12.062>.
- [95] Z.-J. Xu, S. Yang, G.-H. Hu, Q.-H. Wang, J.-R. Li, Numerical study of flow distribution uniformity for the optimization of gradient porosity configuration of porous copper fiber sintered felt for hydrogen production through methanol steam reforming micro-reactor, *Int. J. Hydrogen Energy*. 43 (2018) 4355–4370, <https://doi.org/10.1016/j.ijhydene.2018.01.083>.
- [96] W. Zhou, W. Yu, Y. Ke, Y. Liu, S. Wan, J. Lin, Size effect and series-parallel integration design of laminated methanol steam reforming microreactor for hydrogen production, *Int. J. Hydrogen Energy*. 43 (2018) 19396–19404, <https://doi.org/10.1016/j.ijhydene.2018.08.199>.
- [97] Q. Wu, Y. Wang, D. Mei, S. Si, Development of methanol steam reforming microreactor based on stacked wave sheets and copper foam for hydrogen production, *Int. J. Hydrogen Energy*. 47 (2022) 6282–6294, <https://doi.org/10.1016/j.ijhydene.2021.11.221>.
- [98] S. Zhou, Y. Zhong, W. Lin, H. You, X. Li, L. Wu, W. Zhou, Design and performance evaluation of flexible tubular microreactor for methanol steam reforming reaction, *Int. J. Hydrogen Energy*. 47 (2022) 36022–36031, <https://doi.org/10.1016/j.ijhydene.2022.08.194>.